Proceedings

of the

Workshop

on

Cardiovascular-Respiratory Control

Modeling

organized by

Special Research Center for Optimization and Control

Departments of Mathematics and Physiology
University of Graz

Graz, Austria, June 14 - 16, 2001

Editors
J. Batzel M. Fink D. Schneditz

Introduction

The Cardiovascular-Respiratory Control Group of the Special Research Center for Optimization and Control at the University of Graz, Mathematics Department, offered the workshop

"Issues in Cardiovascular-Respiratory Control Modeling"

on June 14-16 2001. The goal of this workshop was to bring together experts from physiology, dynamical systems, and non-linear control theory focusing on aspects of the cardiovascular and respiratory systems. The group consisted of 33 researchers from 10 countries, broadly balanced between physiologists with a mathematical background and mathematicians with interest in biomedical applications.

Workshop Participants

- David Auerbach (University of Graz, Austria)
- Mostafa Bachar (University of Graz, Austria)
- Jerry Batzel (University of Graz, Austria)
- Gilbert Chauvet (Univ. of Paris V, France)
- Gari Clifford (Oxford Univ., Great Britain)
- Martin Fink (University of Graz, Austria)
- Andrew Fowler (Oxford Univ., Great Britain)
- Michael Guevara (McGill Univ., Canada)
- Dirk Hoyer (Friedrich Schiller Univ., Jena, Germany)
- Eunok Jung (Oak Ridge National Laboratories, U.S.A.)
- Franz Kappel (University of Graz, Austria)
- Thomas Kenner (University of Graz, Austria)
- Armin Leuprecht (Technical Univ. Graz, Austria)
- Alessandro Monti (INRIA, Chesnay, France)
- Robert Nette (Univ. Hospital Rotterdam-Dijkzigt, Netherlands)
- Abraham Noordergraaf (Univ. of Penn., U.S.A.)
- Johnny Ottesen (Roskilde Univ., Denmark)
- Alexander Panfilov (Utrecht Univ., Netherlands)
- Roland Pilgram (University of Graz, Austria)
- Michael Rosenblum (Univ. of Potsdam, Germany)
- Loring Rowell (Univ. of Washington, U.S.A.)
- Daniel Schneditz (University of Graz, Austria)
- Wolfgang Schreiner (Univ. of Vienna, Austria)

Workshop Participants (continued)

- Vito Starc (Univ. of Ljubljana, Slovenia)
- Aneta Stefanovska (Univ. of Ljubljana, Slovenia)
- Hien Tran (North Carolina State Univ., U.S.A.)
- Janos Turi (Univ. Texas, Dallas, U.S.A.)
- Mauro Ursino (Univ. of Bologna, Italy)
- Peter Wabel (Technical Univ. Darmstadt, Germany)
- Nico Westerhof (Free Univ. Amsterdam, Netherlands)
- Robert Zietse (Univ. Hospital Rotterdam-Dijkzigt, Netherlands)
- Ulrich Zwiener (Friedrich Schiller Univ., Jena, Germany)

Proceedings table of contents

Gilbert Chauvet
E-Mail: chauvet@bmsrs.usc.edu

Centre de Recherches en Biologie Intégrative
Hôp. Tarnier-Cochin
University of Paris V;
Dept. Biomedical Engineering
USC, Los Angeles

On the integration of physiological systems; the example of respiratory function

Introduction: the n-level field theory

A crucial problem in physiology is the determination of couplings between organism sub-systems. Because a complex system is composed of interacting parts, a unique formalism is needed which can involve the whole system as well as its components. Another difficulty results from the hierarchical nature of the biological system, which requires traversing levels of organization. Why considering hierarchical systems? In biology, structural hierarchy appears clearly in the usual schema: nucleus, cell, tissue, organ, organism. However, constraints appear because functional processes evolve in a hierarchical structural system. We may note that traversing levels of organization corresponds to a *structural discontinuity*, i.e. a structural border between distinct functional processes. So, the hierarchy describes a specific physiological process at each level, of course coupled with processes evolving in adjacent levels. We have proposed to describe these systems in terms of functional interactions from a source to sinks, with transformations in the sink which correspond to distinct functional process (Chauvet, 1993a). This is the case of the transport of a molecule through the membrane of the target cell.

Structural discontinuities result in the *non-locality* of the global functional processes (Chauvet, 1993b). In a space without structural discontinuity, processes are local, however, giving rise to non homogeneous structures (e.g. chemical reactions far from equilibrium (Prigogine, 1971)). The non-local process allows for the passage from a structure in which phenomena are local to another in which phenomena are also local. Then, the difficulty of the formalized description results from this discontinuity in which functional processes are different and necessary to the transport of the interaction.

The S-Propagator formalism

A new formalism, called *S-Propagator formalism* (Chauvet, 1996, 1998), has been proposed to study the dynamics of hierarchical physiological systems, i.e. to traverse levels of organization. We have shown that the dynamics depend on operators that correspond to the usual models that describe elementary physiological mechanisms.

Briefly, recall that the general n-level field equation which corresponds to an identical diagram for any physiological function is:

$$\begin{aligned}\frac{\partial \Psi^r}{\partial t}(r,t) &= \nabla_r \left(D^r \nabla_r \Psi^r(r,t)\right) + \\ &\int_{D_r(r)} \rho^r(r') \left[P\Psi(r)\right] P(r')\Psi^r \left(r', t - \frac{d(r',r)}{v^r}\right) dr' + \Gamma_r(r,t) \quad (1)\end{aligned}$$

In this equation, Ψ^r is the field variable, $D_r(r)$ is the domain for the structural units at r' connected with r, with density $\rho^r(r')$. $P\Psi(r)$ and $P(r')$ are operators specific to each particular physiological function. v^r is the velocity of the transport from r' to r. The approach proposed here for the integration of coupled physiological systems is based on the representation of the biological system in terms of *non-local* functional interactions Ψ^r between the structural units. The non-local operator H is then associated with the interaction, which represents the transport of matter from one point to another, such that the corresponding equation is a field equation: $H\Psi^r = \Gamma$ where Ψ^r is the field variable and Γ is the local source. The non-local operator H_I is expressed in terms of the S-Propagator that is the product of specific operators P describing the passage of the interaction through the levels of organization. Each operator may be analytically described by a specific model with appropriate assumptions for the specific experiment to interpret. The same type of equation (1) is valid at each level, and is associated with a set of differential equations including those expressed by operators P. An important advantage of this formalism is the ability to describe physiological systems in the same framework. All the concepts may be condensed using a 3D representation in which the x-axis stands for time scales (functions), the z-axis for space scales (structures), and the y-axis for the structural units. Thus, a physiological function corresponds to a given time scale and, in this plane, the levels of structure are distributed on the vertical axis. This general representation is very helpful for the study of hierarchical coupled physiological systems.

The respiratory function in terms of functional interactions

In the example considered here, the pulmonary function may be represented in terms of two levels of structural organization and two levels of functional organization.

The 2 levels of structural organization are denoted as r, s standing for the r-space, the set of *respiratory* units composed of the *ventilatory* units located at r' and the *capillary* units located at r; and for the s-space, the set of *alveolocapillary* units (alveolar sacs) with the alveolocapillary membrane (the *structural discontinuity*). There is only one time scale for these levels. There are 2 levels of functional organization corresponding to two functions: on one hand, ventilation and circulation (the time scale is given by the velocity of propagation in bronchii and vessels), on the other hand, the transport from one terminal bronchiole (i.e. the respiratory lobule) to another through alveolar sacs and the corresponding capillaries (the time scale of these processes corresponds to diffusion, i.e. smaller than the previous one). In this paper only this second function, which is the alveolo-capillary transport will be considered, and I will present briefly the method, i.e. successively: geometrical and topological model, diagrams, equations and operators.

1. *The geometrical and topological model.* Figure 1 shows the respiratory lobule and the corresponding geometrical model.

2. *The S-Propagator diagram* of the respiratory unit may then be derived from the general theory for the function *alveolocapillary transport* (Fig. 2), where $c(r,t)$ is the field variable (O2 or CO2 concentration).

3. *The equation for O2 or CO2 transport* is now derived from the general field equation (1):

$$\begin{aligned}\frac{\partial c}{\partial t}(r,t) &= \nabla_r(D^r \nabla_r c(r,t)) + \\ &\int_{D_r(r)} \rho(r')[P\Psi(r)]P(r')c(r', t - \frac{d(r',r)}{v})dr' + \Gamma_r(r,t) \quad (2)\end{aligned}$$

where v is the velocity of blood. In this equation, c is the field variable, e.g. the dioxide concentration in lung capillaries, and P is the propagator at the lower level, i.e. in this example the transport of O2 molecules from alveolar bags at s' where the concentration is $c(s',t)$ into the current bag where the concentration is $c(s,t)$, then across the membrane and on the vascular side.

Once operators $P\Psi$ and P are expressed as specific local models, the field equation (2) may be solved numerically using routines identical to those used for the general field equation. A new interpretation of the observed phenomenology is then suggested. The same method, based on a unique framework, and applied in the same way to the respiratory system, the nervous system, and their couplings, leads to integrating different functions in terms of their functional interactions. Because of its 3D representation according to time scales, space scales and structural units, this new formalism constitutes a help for the study of very complex systems as the control and regulation in respiratory function.

References

1. Chauvet, G.A. (1993a). *Hierarchical functional organization of formal biological systems: a dynamical approach. I. An increase of complexity by self-association increases the domain of stability of a biological system.* Phil. Trans. Roy. Soc. London B, 339, 425-444.

2. Chauvet, G.A. (1993b). *Hierarchical functional organization of formal biological systems: a dynamical approach. III. The concept of non-locality leads to a field theory describing the dynamics at each level of organization of the (D-FBS) subsystem.* Phil. Trans. Roy. Soc. London B, 339, 463-481.

3. Chauvet, G.A. (1996). *Theoretical Systems in Biology: Hierarchical and Functional Integration.* Volume III: Organisation and Regulation. Oxford: Pergamon.

4. Chauvet, G.A. (1998) *S-propagators : a formalism for the hierarchical organization of physiological systems. application to the nervous and the respiratory systems*, Int. J. General Systems, 28(1), pp. 53-96 (1999).

5. Prigogine, I., Nicolis, G. (1971) *Biological order,structure and instabilities*, Quart. Rev Biophys., 4, 107-148.

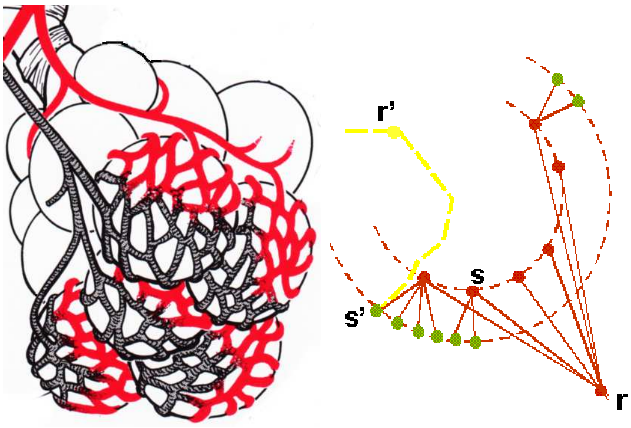

Figure 1: *The respiratory lobule.* Left: anatomical schema; right: corresponding geometrical model, with : r' = location of terminal bronchiole ; r = convergence point of the pulmonary arterioles ; s = convergence point of the capillaries in a given alveolus connected with r ; s' = location of an alveolar sac connected with r'. *These convergences give rise to linear summation of flows.*

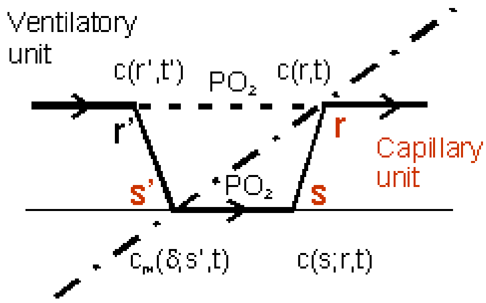

Figure 2: S-Propagator diagram of the respiratory unit

Andrew Fowler
E-Mail: fowler@maths.ox.ac.uk

Dept. of Mathematics
Oxford University

Respiratory control and the onset of periodic breathing

Introduction

Periodic breathing (PB) denotes the clinical observation of rhythmic fluctuations of respiration over a time-scale of the order of tens of seconds to a few minutes. This is due to (and conversely, causes) corresponding changes in the respiratory blood gases (oxygen and carbon dioxide). Cardiovascular changes (measured, for instance, by blood flow in the major vessels) are a natural accompaniment to PB, due to the physiological interaction of these processes. PB is said to have been recognised by Hippocrates though the modern descriptions are attributed to the Irish physicians John Cheyne and George Stokes in the 19th century. PB may be a feature of severe disease of the heart and/or nervous system, but is also a normal feature in preterm infants, healthy elderly subjects during sleep, and adults taken to high altitude (see Tobin and Snyder (1984) or Yamashiro and Kryger (1993) for reviews).

The control of respiration over PB time-scales is effected by two sets of chemoreceptors, one in the brainstem (that responds exclusively to CO_2), and the other in the carotid body (that responds to both O_2 and CO_2). Instability in these feedback control loops is thought to underlie the oscillations that constitute PB (Cherniack and Longobardo 1986); this is the conceptual framework for a number of mathematical models (Mackey and Glass 1977, Khoo *et al.* 1982, Carley and Shannon 1988, Longobardo *et al.* 1989, ElHefnawy *et al.* 1990, Batzel and Tran 2000), including ours (Fowler *et al.* 1993, Fowler and Kalamangalam 2000). These various models are conceptually similar, and range from the simple but appealing (Mackey and Glass 1977) to the complicated but opaque (Grodins *et al.* 1967). In this abstract we compare the Mackey-Glass model with a reduced version of the Grodins model.

The Mackey-Glass model

The arterial blood flow from the lungs carries CO_2 at partial pressure p. The CO_2 is provided as a waste product by metabolism in the tissues at a rate M, and removed at a rate pV, where V is the ventilation. It is assumed that ventilation is controlled only by the central chemoreceptor in the brain. The Mackey-Glass model is then

$$K\frac{dp}{dt} = M - pV, \tag{1}$$

describing the change of CO_2 partial pressure in a single compartment of volume K. One can think of this compartment as representing the lungs, whereas the more complicated Grodins model has three principal compartments (lungs, tissue, brain). The model is completed by a recipe for the ventilation controller, taken as

$$V = V(p_\tau), \tag{2}$$

where $p_\tau = p(t-\tau)$, and τ is the delay arising from arterial blood transport between the lungs and the brain.

The controller function is monotone increasing, and more or less linear in hypercapnia (Cunningham *et al.* 1986). There is a unique steady state $p = p^*$ (≈ 40 mm Hg) in which $M = p^* V(p^*)$, whose stability is determined by writing

$$p = p^* + \tilde{p}, \tag{3}$$

and linearising (1), by virtue of the supposition that $\tilde{p} \ll 1$, to obtain

$$K\frac{d\tilde{p}}{dt} = -V^*\tilde{p} - p^* G\tilde{p}_\tau, \tag{4}$$

where

$$V^* = V(p^*), \quad G = V'(p^*) \tag{5}$$

are the resting ventilation and controller gain. Solutions of the form $\exp(\sigma t)$ exist, provided

$$K\sigma = -\left[V^* + p^* G e^{-\sigma\tau}\right], \tag{6}$$

and one can show that oscillatory (Hopf) instability occurs if

$$\frac{\tau p^* G}{K} \gtrsim \frac{\pi}{2}, \tag{7}$$

and the resulting oscillations have period $\approx 4\tau$.

The Mackey-Glass theory is conceptually pleasing, and is qualitatively consistent with the occurrence of periodic breathing in stroke (increased gain G) or heart failure (increased delay τ), but Mackey and Glass had to choose slightly imaginative values for instability to occur. They chose $M/K = 6$ mm Hg min^{-1}, $V^* = 7$ l min^{-1}, $G = 4$ l min^{-1} mm Hg^{-1}, for which instability occurs if $\tau > 27$ seconds. This corresponds to a threefold decrease in normal cardiac output, but normal values of G and M/K are lower by factors of about two. Moreover, the corresponding predicted periods (two minutes) are too long.

The Grodins model

The model enunciated by Grodins et al. (1967) describes the blood gas concentrations in four separate compartments, namely brain, (other) tissues, lungs and cerebro-spinal fluid. Concentrations of CO_2, O_2 (and N_2) are described by conservation laws which balance the transport between compartments via arteries or veins with the metabolic consumption or production rates (of O_2 and CO_2 respectively). In seeking to understand this model, we begin by focussing on the transport of CO_2 only, and we also ignore complications associated with variable blood flow.

Three equations describing CO_2 levels in the lung, brain and tissue compartments are Grodins et al.'s (1967) equations (1.1), (1.4) and (1.7), here written in terms of partial pressures assuming a (locally) linear buffering relation between CO_2 concentrations

C and partial pressures P, $\partial C/\partial P = K_{\mathrm{CO_2}}$:

$$\begin{aligned}
K_{\mathrm{L}}\dot{P}_{\mathrm{aCO_2}} &= -VP_{\mathrm{aCO_2}} + 863K_{\mathrm{CO_2}}Q[P_{\mathrm{vCO_2}} - P_{\mathrm{aCO_2}}], \\
K_{\mathrm{CO_2}}K_{\mathrm{B}}\dot{P}_{\mathrm{CO_2}} &= MR_{\mathrm{BCO_2}} + K_{\mathrm{CO_2}}Q_{\mathrm{B}}[P_{\mathrm{aCO_2}}(t-\tau_{\mathrm{aB}}) - P_{\mathrm{BCO_2}}] \\
&\qquad\qquad -D_{\mathrm{CO_2}}[P_{\mathrm{BCO_2}} - P_{\mathrm{CSFCO_2}}], \\
K_{\mathrm{CO_2}}K_{\mathrm{T}}\dot{P}_{\mathrm{TCO_2}} &= MR_{\mathrm{TCO_2}} + \\
&\qquad (Q-Q_B)K_{\mathrm{CO_2}}[P_{\mathrm{aCO_2}}(t-\tau_{aT}) - P_{\mathrm{TCO_2}}].
\end{aligned} \tag{8}$$

In the above three equations referenced by (8), suffixes a, L, B, T, v, CSF refer to arterial, lung, brain, tissue, venous and cerebro-spinal fluid values. Alveolar values are taken equal to arterial values, K denotes volume (of lungs, etc.), MR is metabolic $\mathrm{CO_2}$ production rate, V is the ventilation rate, and inspired $\mathrm{CO_2}$ is assumed zero. The numerical factor 863 arises through the conversion of STP dry gas volumes to BTP saturated values (West 1990). The delays τ_{aB} and τ_{aT} arise through the transport time of the blood flow Q through the body: Q_B to the brain, $Q - Q_B$ to the (other) tissues. In addition, we have

$$QP_{\mathrm{vCO_2}} = Q_{\mathrm{B}}P_{\mathrm{BCO_2}}(t-\tau_{\mathrm{vB}}) + (Q-Q_{\mathrm{B}})P_{\mathrm{TCO_2}}(t-\tau_{\mathrm{vT}}); \tag{9}$$

τ_{vB} and τ_{vT} are the corresponding venous delays. The brain-CSF transport term proportional to $D_{\mathrm{CO_2}}$ is small with Grodins' choice of parameters, and will be ignored here, although this may be dangerous, since it is actually the case that the central chemoreceptor responds to changes in pH of the CSF induced by this term (West 1990).

We can see that the first equation in (8) corresponds to the Mackey-Glass equation, and we might expect that the Grodins model would reduce to the Mackey-Glass model if the second and third equations in (8) were fast. Specifically, if the $P_{\mathrm{TCO_2}}$ equation is fast, if $Q_B \ll Q$, and if $\tau_{aT} + \tau_{vT}$ is small, then the Mackey-Glass model can be recovered, with $M = 863MR_{\mathrm{TCO_2}}$. As we shall see, only the second of these assumptions is valid.

Reduced, dimensionless models

We write partial pressures in terms of a typical arterial $\mathrm{CO_2}$ partial pressure of $P^* =$ 40 mm Hg; more specifically, we define (mysteriously; time is short)

$$\begin{aligned}
P_{\mathrm{aCO_2}} &= P^*[1+\varepsilon p_a], & P_{\mathrm{BCO_2}} &= \frac{MR_{\mathrm{BCO_2}}}{K_{\mathrm{CO_2}}Q_B} + P^*[1+\frac{\varepsilon}{\gamma}p_B] \\
P_{\mathrm{TCO_2}} &= P^*[1+\varepsilon+\varepsilon p_T], & P_{\mathrm{vCO_2}} &= P^*[1+\varepsilon(1+p_v)].
\end{aligned} \tag{10}$$

In addition, we write time in terms of a time scale $K_B/Q_B \approx \frac{4}{3}$ min (80 s); note that this is comparable to a typical oscillation period in periodic breathing. We assume Q and Q_B are constant. Finally, we suppose that the controller function V depends only on $P_{\mathrm{BCO_2}}$. Typical ventilatory responses in hypercapnia are linear, of the form

$$V = G\left[P_{\mathrm{BCO_2}} - \left(\frac{MR_{\mathrm{CO_2}}}{K_{\mathrm{CO_2}}Q_B} + I_C\right)\right]_+, \tag{11}$$

with apnea ($V = 0$) occurring below an arterial threshold I_C. The notation $[x]_+$ means $\max(x, 0)$. (The odd choice of threshold in (11) is made so that I_C corresponds to the value of alveolar P_{CO_2} at apnea in the steady state.) The dimensionless Grodins model is then (ignoring brain–CSF transport)

$$
\begin{aligned}
\frac{1}{\Lambda}\dot{p}_a &= 1 + p_v - p_a - (1 + \varepsilon p_a)[1 + p_B]_+, \\
\dot{p}_B &= \gamma p_a(t - \tau_{aB}^*) - p_B, \\
\dot{p}_T &= s[p_a(t - \tau_{aT}^*) - p_T], \\
p_v &= p_T(t - \tau_{vT}^*) + \delta[c + \gamma^{-1} p_B(t - \tau_{vB}^*) - p_T(t - \tau_{vT}^*)].
\end{aligned}
\tag{12}
$$

The parameters appearing in these equations are defined, and have typical values as follows:

$$
\begin{aligned}
\delta &= \frac{Q_B}{Q} \approx 0.13, \\
\Lambda &= \frac{863 K_{\mathrm{CO}_2} Q K_B}{K_L Q_B} \approx 11.5, \\
\varepsilon &= \frac{MR_{\mathrm{TCO}_2}}{K_{\mathrm{CO}_2} P^* (Q - Q_B)} \approx 0.16, \\
s &= \frac{(Q - Q_B) K_B}{K_T Q_B} \approx 0.18, \\
\gamma &= \frac{G P^*}{863 K_{\mathrm{CO}_2} Q} \approx 2.78, \\
c &= \frac{MR_{\mathrm{BCO}_2}}{MR_{\mathrm{TCO}_2}} \left(\frac{Q}{Q_B} - 1 \right) - 1 \approx 1,
\end{aligned}
\tag{13}
$$

and the dimensionless delays are defined by

$$
\tau_{aB}^* = \frac{V_{aB}}{K_B} \approx 0.14, \quad \tau_{aT}^* = \frac{V_{aT}}{K_B} \approx 0.24, \quad \tau_{vT}^* = \frac{V_{vT}}{K_B} \approx 0.44, \quad \tau_{vB}^* = \frac{V_{vB}}{K_B} \approx 0.08, \tag{14}
$$

where $V_{aB}, V_{aT}, V_{vT}, V_{vB}$ are essentially blood vessel volumes. Reduction to the Mackey-Glass equation requires $\Lambda \ll 1$, but we see that in fact the opposite is the case.

The magic bit is this: $\Lambda \gg 1$, so p_a rapidly approaches and stays in quasi-equilibrium. With $\varepsilon \ll 1$, this implies

$$
p_a \approx 1 + p_v - [1 + p_B]_+. \tag{15}
$$

Next, $\delta \ll 1$, so that $p_v \approx p_T(t - \tau_{vT}^*)$. Hence, p_T and p_B satisfy, approximately, a pair of coupled differential-delay equations, with $\dot{p}_B \sim \gamma$ and $\dot{p}_T \sim s$. Since $s \ll \gamma$, p_T is slowly varying. For bounded p_B, p_T will be approximately constant, and we can take its value to be zero, by specific choice of P^* (one can show that $P^* = \gamma I_C / (\gamma - \varepsilon)$): the Grodins model is then reduced to the first order equation

$$
\dot{p_B} = \gamma[1 - \{1 + p_B(t - \tau_{aB}^*)\}_+] - p_B. \tag{16}
$$

For values of $p_B = O(1)$, we find that variations of P_{BCO_2} are of order $863\, MR_{\mathrm{TCO}_2}/GP^*$ $\approx 2\,\mathrm{mm\,Hg}$.

Linear stability

Equation (16) may serve as a simple Grodins paradigm which can be contrasted with the Mackey-Glass paradigm. Instability occurs when γ is large, and can be analysed as before. We find that instability occurs for

$$\gamma \gtrsim \gamma_c = \frac{\pi}{2\tau^*_{aB}} \approx 11.2 \tag{17}$$

(the exact critical value is 11.865 when $\tau^*_{aB} = 0.14$) and the period of oscillations is approximately $4\tau^*_{aB}$. In terms of dimensional quantities, the oscillation period is approximately

$$t_p \approx \frac{4V_{aB}}{Q_B} = 4\tau_{aB}. \tag{18}$$

The instability criterion can be written as

$$\frac{V_{aB}GP^*}{K_BQ} \gtrsim \frac{863K_{\mathrm{CO}_2}\pi}{2} \approx 6.8, \tag{19}$$

This criterion can be directly compared to the Mackey-Glass result (7), bearing in mind that $\tau_{aB} = V_{aB}/Q_B$. Based on standard values, our estimate for γ is 2.78. We thus see that either a four fold increase in G, or a four fold decrease in cardiac output, can lead to periodic breathing. The first of these conditions is associated with stroke, and the second with congestive heart failure. Although the Grodins model finds it easier to produce instability than the Mackey-Glass model, it still seems to require severe changes in G or Q. If such severity is unrealistic, then other physiological effects must be considered, such as the rôle of vasodilation in maintaining cerebral circulation, the rôle of other compartments in the circulation, and the details of the central controller dependence on pH in the CSF. Of course, the rôle of oxygen and of the peripheral controller also needs to be addressed.

References

1. Batzel, J. J. and H. T. Tran 2000 Modeling instability in the control system for human respiration: applications to infant non–REM sleep. Appl. Math. Comput. **110**, 1–51.

2. Carley, D. W. and D. C. Shannon 1988 A minimal mathematical model of human periodic breathing. J. Appl. Physiol. **65**, 1400–1409.

3. Cherniack, N. S. and G. S. Longobardo 1986 Abnormalities in respiratory rhythm. In: Handbook of Physiology; Section 3, The respiratory system; Volume II; Control of breathing, part 2, eds. N. S. Cherniack and J. G. Widdicombe, pp. 729–749, American Physiological Society.

4. Cunningham, D. J. C., P. A. Robbins and C. B. Wolff 1986 Integration of respiratory responses to changes in alveolar partial pressures of CO_2 and O_2 and in arterial pH. In: Handbook of Physiology; Section 3, The respiratory system; Volume II; Control of breathing, part 2, eds. N. S. Cherniack and J. G. Widdicombe, pp. 475–528, American Physiological Society.

5. ElHefnawy, G. M., E. N. Bruce, and N. S. Cherniack 1990 Stability analysis of CO_2 control of ventilation. J. Appl. Physiol. **69**, 498–503.

6. Fowler, A. C., G. P. Kalamangalam and G. C. Kember 1993 A mathematical analysis of the Grodins model of respiratory control. IMA J. Math. Appl. Med. Biol. **10**, 249–280.

7. Fowler, A. C. and G. P. Kalamangalam 2000 The role of the central chemoreceptor in causing periodic breathing. IMA J. Math. Appl. Med. Biol. **17**, 147–167.

8. Grodins, F. S., J. Buell and A. J. Bart 1967 Mathematical analysis and digital simulation of the respiratory control system. J. Appl. Physiol. **22**, 260–276.

9. Khoo, M. C. K., R. E. Kronauer, K. P. Strohl and A. S. Slutsky 1982 Factors inducing periodic breathing in humans: a general model. J. Appl. Physiol. **53**, 644–659.

10. Longobardo, G. S., B. Gothe and N. S. Cherniack 1989 Factors affecting respiratory system stability. Ann. Biomed. Eng. **17**, 377–396.

11. Mackey, M. C. and L. Glass 1977 Oscillations and chaos in physiological control systems. Science **197**, 287–289.

12. Tobin, M. J. and S. V. Snyder 1984 Cheyne-Stokes respiration revisited: controversies and implications. Critical Care Medicine **12**, 882–887.

13. Yamashiro, Y. and M. H. Kryger 1993 Review: Sleep in heart failure. Sleep **16**, 513–523.

14. West, J. B. 1990 Respiratory physiology: the essentials, 4th edition, Williams and Wilkins, Baltimore.

A. C. Fowler
Mathematical Institute, Oxford University
24–29 St. Giles'
Oxford OX1 3LB, England

Dirk Hoyer and Ulrich Zwiener
E-Mail: idh@mti.uni-jena.de and uzwi@mti-n.uni-jena.de

Institute for Pathophysiology
Friedrich Schiller University

Evaluation of different types of cardiovascular-respiratory interdependencies - approaches by mutual information and phase synchronisation statistics

The heart rate variability (HRV) is related to several mechanisms of the complex cardiovascular coordinations such as respiratory heart rate modulation and several other interactions. The underlying processes and couplings are basically nonlinear. Essential aspects of those behaviors are phase synchronization mechanisms between coupled nonlinear oscillators and the complex dynamics of multi-matched control loops with regard to different physiological object functions. In order to understand and quantitatively assess those physiological interactions an adequate coupling analysis is necessary.

Mutual Information

In classical power spectral and coherence analysis the linear characteristics and dependencies of oscillatory processes are considered. This is a useful approximation in many cases, but with regard to complex coordinations an obviously limited, in some cases even insufficient approach. In contrast, mutual information can basically consider any type of statistical dependencies. Mutual information $I(\xi, \eta)$ describes the amount of information on a given random quantity η we can obtain from the observation of another quantity ξ. When applied to a pair of signals $[\xi(t),\eta(t)]$ mutual information provides a quantification of the coupling between these signals. Mutual information quantifies both linear and non-linear statistical dependencies. This can be done as function of a time delay corresponding to the well known correlation functions. Mutual information characterizes properties basically different from linear correlation and power spectra/coherence analysis.

We investigated Auto Mutual Information Functions (AMIF) of separate cardiovascular-respiratory quantities, such as heart rate, respiration, and arterial blood pressure. Cross Mutual Information Functions (CMIF) were investigated with regard to the interdependencies between the respective pairs, such as between respiration and heart rate, and so on. This was done in several experimental measurements of pathophysiologically disturbed cardiovascular coordinations.

Phase Dependencies and Synchronizations

Phase synchronizations inevitably appear in neuronal oscillators because of the phase dependencies of integrate and fire mechanisms. This was shown in different examples starting from the cellular level up to global cardiovascular-respiratory processes, such as between respiratory movements, blood pressure, and heart beats. Those phase interdependencies between the heart beat cycles and the respiratory cycles during different physiological situations were quantitatively assessed by means of histogram statistics and dynamic properties of the instantaneous phase differences and statistically confirmed by testing phase randomized surrogate data. This behavior is furthermore part of the complex dynamics based on the multi-matched control loops. The physiological interpretation of phase synchronizations in terms of "relative coordination", "multi-stabilization", "energy consumption optimization", or "information processing efficiency" is a currently outstanding question of interest.

The presented approaches belong to our concept of analysing nonlinear and complex coordinations within the cardiovascular-respiratory system, in particular between heart rate, respiration, and blood pressure.

Research Topics and Interests in Cooperations

We are interested in any type of scientific cooperation such as: exchange of experiences, data, methods, persons, and common projects.

- **Research Interests:** - Nonlinear dynamics and coordinations - Cardiovascular system (heart rate, respiration, blood pressure) - Normal behavior and under physical load - Pathophysiologically disturbed behavior: nonlinear components of heart rate variability, and cardiopulmonary and cardiovascular interactions in different pathogenetic states, such as myocardial infarction, heart failure, septic shock, multi-organ dysfunction syndrome, and severe brain disorders - Evaluation of functional structure of nonlinearities in dynamics of heart rate, respiration, blood pressure und there interactions.
- **Methods:** - Uni- and multivariate time series analysis - Standard methods (time and frequency domain) of HRV-analysis as reference - Nonlinear predictions - Mutual information, entropy - Phase synchronizations - Data - Experimental data of pathophysiologically well defined states (rats, ...) - Clinical data of patients.
- **Projects:** - Complexity and nonlinear coordination of cardiovascular dynamics (heart rate, respiration, blood pressure, and their couplings): - Brain damaged patients - Multi-Organ Dysfunction Syndrome (MODS) - Sepsis - Nonlinearities and coordinations of heart rate variability and blood pressure fluctuations depending on autonomic blockades and pathophysiological influences (rats) - Nonlinear fetal heart rate dynamics - maturation and pathophysiological disturbances (fetal magnetocardiography) - Nonlinear heart rate dynamics in heart failure patients

Dr.-Ing. habil. Dirk Hoyer,
Systems analysis group, Institute for Pathophysiology,
Friedrich-Schiller University, Jena

Prof.Dr.med. Dr.phil. Ulrich Zwiener,
Head of the Institute for Pathophysiology,
Friedrich-Schiller University, Jena

References

1. Zwiener U, Hoyer D, Luethke B, Schmidt K, Bauer R (1995) Relations between parameters of spectral power densities and deterministic chaos of heart rate variability. J Autonom Nerv System 25 : 132-135

2. Hoyer D, Schmidt K, Zwiener U, Bauer R (1996) Characterization of complex heart rate dynamics and their pathological disorders by nonlinear prediction. Cardiovasc Res 31 : 434-440

3. Zwiener U, Hoyer D, Bauer R, Luethke B, Walter B, Schmidt K, Hallmeyer S, Kratzsch B, Eiselt, M. (1996) Deterministic-chaotic and periodic properties of heart rate and arterial pressure fluctuations and their mediation in piglets. Cardiovasc Res 31 : 455-465

4. Hoyer D, Hader O, Zwiener U (1997) Relative and intermittent cardiorespiratory coordinations. IEEE Engineering and Medicine and Biology 16 : 97-104

5. Hoyer D, Liebovitch LS, Schmidt K, Luethke B, Zwiener U (1997) Practical problems of determining the dimension from heart rate data. Medical and Biological Engineering and Computing 35 : 27-32

6. Pompe P, Blidh P, Hoyer D, Eiselt M (1998) Measuring the coupling in the cardiorespiratory system using mutual information. IEEE Engineering in Medicine and Biology 17 : 32-39

7. Hoyer D, Kaplan DT, Schaaff F, Eiselt M (1998) Determinism in bivariate cardiorespiratory phase space sets - how to detect nonlinear coordinations. IEEE Engineering in Medicine and Biology 17 : 26-31

8. Hoyer D, Kaplan D, Palus M, Pompe B, Seidel H (1998) New systems-analytical approaches to nonlinear coordination - applications in the cardiorespiratory system. IEEE Engineering in Medicine and Biology 17 : 58-61

9. Palus M, Hoyer D (1998) Surrogate data in detecting nonlinearity and phase synchronization. IEEE Engineering in Medicine and Biology : 17 : 40-45

10. Chon, KH, Hoyer D, Armoundas AA, Holstein-Rathlou NH, Marsh DJ (1999): Robust nonlinear autoregressive moving average model parameter estimation using stochastic recurrent artificial neural networks. Annals of Biomed. Engineering 27 : 538-547.

11. Hoyer D, Hoyer O, Zwiener U (2000): A new approach to uncover dynamic phase coordination and synchronization. IEEE Transactions on Biomedical Engineering 47 : 68-74

12. Hoyer D, Frasch M, Hoyer O, Eiselt M, Zwiener U (2001): Validating phase relations between cardiac and breathing cycles during sleep. IEEE Engineering in Medicine and Biology 20 : 101-106.

13. Zwiener U, Schelenz S, Bramer S, Hoyer D (2001): Short-term dynamics of relative coordination between respiratory movements, heart rate and arterial pressure fluctuations within the respiratory frequency range. Physiological Research 50 : 59-69.

14. Hoyer D, Leder U, Hoyer H, Pompe B, Sommer M, Zwiener U (2002): Mutual Information and phase dependencies: measures of reduced nonlinear cardiorespiratory interactions after myocardial infarction. Medical Engineering and Physics (in press).

Eunok Jung
E-Mail: junge@ornl.gov

Oakridge National Laboratories, Oakridge, Tenn.

2-D Simulations of valveless pumping using the Immersed Boundary Method

Pumping blood in one direction is the main function of the heart, which is equipped with valves that ensure unidirectional flow. Is it possible, though, to pump blood without valves? This research is intended to show by numerical simulation the possibility of a net flow which is generated by a valveless mechanism in a circulatory system. Simulations of valveless pumping are motivated by physical experiments of Kilner [4], which had been developed from experiments by Liebau [5,6,7]. They observed net flow in one direction which depends on the location of periodic forcing in his experiments. We have examined flows driven by pumping without valves in Liebau's model, a loop of tubing of which part is almost rigid and the other part is flexible. In agreement with experiments, we find that net flow can indeed be driven around such a loop by periodic forcing at one location, but we also find something new: the direction of the flow depends on the driving frequency of the periodic forcing.

One of the applications of valveless pumping may turn out to be cardiopulmonary resuscitation (CPR). The blood flow during CPR has been explained by two theories: the thoracic pump and cardiac compression mechanisms. In support of the thoracic pump model, it has been reported that the heart is "a passive conduit for blood flow" during chest compression, with an open mitral valve throughout the cardiac cycle and anterograde (forward) transmitral blood flow even during chest compression [1,2]. Despite the observed lack of valve function, some patients with cardiac arrest are successfully resuscitated by external chest-compression CPR. These findings are controversial, however. Other investigators who favor the cardiac compression theory believe that the heart acts as a pump and its valves function normally. It is possible, of course, that both theories are correct, each in a different set of circumstances. Our computational model of valveless pumping might be applicable to the thoracic pump model and help to understand the thoracic pump mechanism. If the magnitude and even the direction of flow in valveless pumping are indeed frequency dependent, as our results seem to indicate, it is of obvious importance to know what frequency of chest compression will produce the most effective CPR. Another biological example of valveless pumping may occur in the human embryo at the end of the third week of gestation. At this stage of development, the valves of the heart have not yet formed. Nevertheless, there is a net flow in the circulatory system that is somehow generated by the beating of the heart. An industrial application of valveless pumping is in microelectromechanical system (MEMS) devices, where there is a need to produce fluid motion without moving anything inside the fluid. MEMS devices could be built that incorporate flexible flow channels. In that case, our findings might be applicable to the design of valveless pumps for MEMS devices.

The immersed boundary method is used for the mathematical and numerical method. This method is applicable to problems involving an elastic structure interacting with a viscous incompressible fluid. It has been applied to a variety of problems, particularly in biophysics, including two-dimensional and three-dimensional simulations of blood flow in the heart [9,10], the design of prosthetic cardiac valves, platelet aggregation during blood clotting, wave propagation in the cochlea, the flow of suspensions, peristaltic pumping of solid particles, and aquatic animal locomotion. The philosophy of the immersed boundary method is that the elastic material is treated as a part of the fluid in which singular forces are applied. The fluid and the elastic immersed boundary constitute a coupled mechanical system: The motion of the fluid is influenced by the force generated by the immersed boundary on the fluid, but at the same time the immersed boundary moves at the local fluid velocity and exerts singular forces locally on the fluid. The strength of this method is that it can handle the complicated and time dependent geometry of the elastic immersed boundary which interacts with the fluid, and that it does so while using a fixed regular lattice for the fluid computation.

The following is a summary of the computational method. The motion of a viscous incompressible fluid is represented by Eulerian velocities and pressures on a fixed Cartesian coordinate system and the motion of the elastic materials are expressed in Lagrangian form. A typical time step of the computational method proceeds as follows: At the beginning of the time step, the fluid velocity at each point of the fluid grid and the boundary configuration of the elastic materials are known. The boundary forces are computed from the given boundary configuration, and then used to spread these boundary forces into the nearby fluid grid to evaluate the fluid forces using the Dirac delta function. With the fluid forces known, the Navier-Stokes equations are solved in order to get an updated velocity on the fluid grid. Finally, upon interpolating the updated velocity field to the boundary locations using the same delta function, the boundary is moved at the interpolated velocity. This completes the time step. A detailed description of the Immersed Boundary Method is in [9,10].

The two main results of this paper are as follows: First, a net flow around the loop is produced by the periodic forcing on one end of the flexible boundary, despite the absence of valves. Previous investigators have observed this phenomenon in physical experiments [4], and a theoretical explanation based on a lumped parameter (ODE) model [8] has been proposed, but this is the first time, to our knowledge, that valveless pumping has been demonstrated by a computer simulation based on the Navier-Stokes equations. Second, we find that the direction of flow around the loop is determined not only by the position of the periodic compression but also by the amplitude and frequency of the driving force, see Figures 1 and 2. This is a new, unexpected phenomenon, not previously reported, and the most important prediction of our model. A detailed discussion for our results is in [3].

Preliminary physical experiments performed in the Courant Institute WetLab confirm that the flow can be driven in either direction from the same location depending on the details of the forcing. Experiments will be described in a future publication with Jun Zhang.

We are confident that numerical experiments such as those begun in this paper will help answer many questions about the mechanism of valveless pumping. Even though the results demonstrate success in modeling valveless pumping, there is still much future work that remains to be done, such as giving a theoretical explanation for this mysterious phenomenon, and extending this model to the three-dimensional case in order to make it more realistic and more applicable to real-world biomedical problems, like CPR. Another important part of the future work will be the comparison of computed and experimental results.

References

1. R. P. Beyer, *A computational model of the cochlea using the immersed boundary method*, J. Comput. Phys., 98 (1992), pp. 145-162.

2. J. M. Criley, J. T. Niemann, J. P. Rosborough, S. Ung, and J. Suzuki, *The heart is a conduit in CPR*, Crit. Care Med., 9 (1981), p. 373.

3. E. Jung and C. S. Peskin, *Two-Dimensional Simulations of Valveless Pumping using the Immersed Boundary Method*, SIAM J. on Scientific Computing, Volume 23, pp. 19-45

4. P. J. Kilner, *Formed flow, fluid oscillation and the heart as a morphodynamic pump (abstract)*, European Surgical Research, 19 (1987), pp. 89–90.

5. G. Liebau, *Die Bedeutung der Tragheitskrafte für die Dynamik des Blutkreislaufs*, Zs Kreislaufforschung, 46 (1957), pp. 428-438.

6. G. Liebau, *Die Stromungsprinzipien des Herzens*, Zs Kreislaufforschung, 44 (1955), pp. 677-684.

7. G. Liebau, *Uber ein Ventilloses Pumpprinzip*, Naturwissenschsften, 41 (1954), pp. 327-328.

8. M. Moser, J. W. Huang, G. S. Schwarz, T. Kenner, and A. Noordergraaf, *Impedance defined flow, generalisation of William Harvey's concept of the circulation—*370 *years later*, Internat. J. Cardiovascular Medicine and Science, 1 (1998), pp. 205-211.

9. C. S. Peskin and D. M. McQueen, *A three-dimensional computational method for blood flow in the heart: Immersed elastic fibers in a viscous incompressible fluid*, J. Comput. Phys., 81 (1989), pp. 372-405.

10. C. S. Peskin and D. M. McQueen, *A general method for the computer simulation of biological systems interacting with fluids*, Symposia of the Society for Experimental Biology, 49 (1995), pp. 265-276.

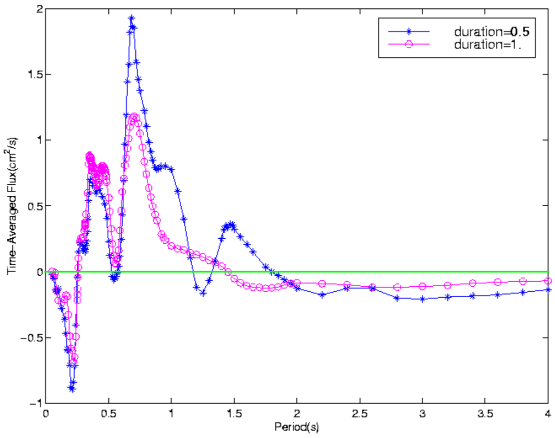

Figure 1: The time-averaged flow around a loop as a function of period (1/frequency): Each data point summarizes a separate numerical experiment of 150 (s). positive flow is clockwise, and negative flow is counter-clockwise. The valveless pumping has a strong dependence on the frequency of the driving oscillation. Indeed, there appear to be resonances at rather specific frequencies, which are most effective in driving the flow in one direction or the other.

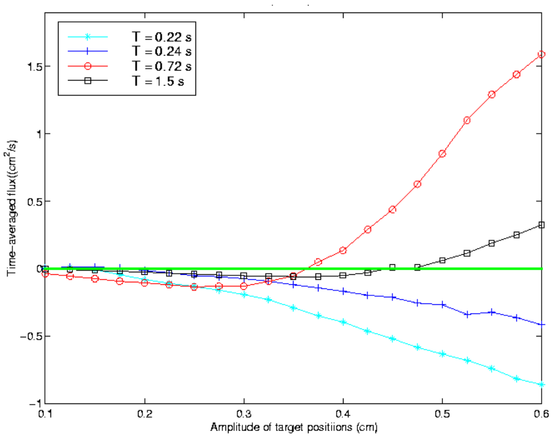

Figure 2: The time-averaged flow around the loop as a function of the amplitude of the driving oscillation: Each data point summarizes a separate numerical experiment of 150 (s). Positive flow values denote clockwise net flow, and negative values denote counterclockwise net flow. For all periods shown, the flow is negative (counterclockwise) at low amplitude, but for some periods (T=0.72 s and T=1.5 s) it reverses and becomes positive (clockwise) at high amplitude.

Armin Leuprecht and Karl Perktold
E-Mail: leu@matd.tu-graz.ac.at

Institute of Mathematics
Graz University of Technology

Computer simulations of blood flow in large arteries

1 Introduction

It is widely accepted that there exists a correlation between local blood flow behavior and the genesis and development of arterial disease. Consequently, the study of hemodynamic phenomena at specific regions in the vascular system has become a field of research world-wide. A deeper understanding of pathological processes can be gained by the mathematical modeling and numerical simulation of the occurring flow effects which is enabled by the significant advances in numerical mathematics and the essentially increased power of computers in the last few years. The application of computer modeling of blood flow provides the opportunity to obtain a full set of hemodynamic data more precisely than by measurement alone. On the other hand a basic requirement for the realistic computational prediction is the anatomically correct modeling [6], because local flow behavior is strongly dependent on geometrical conditions. The first part of this study deals with the simulation of human aortic blood flow where the main features are the anatomically realistic modeling of the complex vessel geometry and the consideration of time-dependent flow domains. Geometry and flow conditions of a human ascending aorta were gained from MRI scans. Blood is described by a Newtonian fluid. In a second part non-Newtonian effects of blood are considered. Basic viscoelastic behavior of blood flow is demonstrated applying a Jeffreys' type model. The numerical approach of the flow problems applies the finite element method.

2 Methods

2.1 Aortic Flow

The geometry of the ascending aorta of a young, healthy, female volunteer has been acquired from MRI scans using a 1.5T whole body MR scanner (Philips Gyroscan NT) [4]. In-plane spatial resolution was $1 \times 1\,mm^2$, and 25 heart phases were recorded every $24,5\,ms$ during a cardiac cycle. A bi-cubic spline algorithm has been developed to create an accurate and smooth model of the vessel wall. The procedure applies axis and surface smoothing in space and periodically in time. After surface generation the volume was filled with more than 300.000 brick elements. Full velocity information was measured at the inlet just downstream of the heart valves (in a distance between 2 and $8\,mm$) and at a cross-section about $6\,cm$ downstream. The measured inflow velocity data was smoothed by spline approximation and incorporated in the computational study as inlet boundary condition. The second measured slice at the beginning of the aortic arch served for validation purposes.

The mathematical description of blood flow uses the time-dependent, three-dimensional, incompressible Newtonian Navier-Stokes equations for Newtonian fluids. Due to the moving flow domain the equations have to be modified applying the *arbitrary Lagrangian-Eulerian* technique with respect to the convective velocity [2]. Neglecting the body forces the equations are written in non-dimensional form:

$$\frac{\partial \mathbf{u}}{\partial t} + \Big((\mathbf{u} - \hat{\mathbf{u}}) \cdot \nabla \Big) \mathbf{u} = \frac{1}{Re} \Delta \mathbf{u} - \nabla p \tag{1}$$

$$\nabla \cdot \mathbf{u} = 0 \tag{2}$$

where $\mathbf{u}$ is the velocity vector, $\hat{\mathbf{u}}$ denotes the domain velocity vector and p is the isotropic pressure. $Re = U_0 L_0 / \nu$ is the Reynolds number, where U_0 denotes the reference velocity, L_0 the reference length and $\nu = \mu / \rho$ the kinematic viscosity as fraction of the constant dynamic viscosity μ and the constant fluid density ρ.

At the flow inlet the MRI measured velocity profiles were used as inflow boundary condition and the no-slip condition was imposed at the vessel walls. At the outlet the traction-free condition (corresponding to fully developed flow) was specified. In order to minimize the influence of this idealized condition the computational domain has been extended to the end of the aortic arch.

The solution of the Navier-Stokes equations is performed numerically using the finite element method. The solution procedure is based on our recently developed velocity-pressure correction method applying Galerkin finite element discretization [3]. Due to the high Reynolds number (convection dominated flow) and high Womersley number occurring in the ascending aorta the numerical scheme has to be stabilized by means of a streamline upwind technique. The resulting algebraic equation systems are solved by means of our recently developed modified bi-conjugate gradient algorithm [1].

2.2 Viscoelastic Flow

The governing equations for a general flow of an Oldroyd-B fluid are described by the Navier-Stokes equations and the constitutive relation:

$$\frac{\partial \mathbf{u}}{\partial t} + (\mathbf{u} \cdot \nabla) \mathbf{u} = \frac{1}{Re} \nabla \cdot \boldsymbol{\tau}_1 + \frac{\eta_2}{\eta_0} \frac{1}{Re} \Delta \mathbf{u} - \nabla p \tag{3}$$

$$\nabla \cdot \mathbf{u} = 0 \tag{4}$$

$$\boldsymbol{\tau}_1 + We \left(\frac{\partial \boldsymbol{\tau}_1}{\partial t} + \mathbf{u} \cdot \nabla \boldsymbol{\tau}_1 - \boldsymbol{\tau}_1 \cdot \nabla \mathbf{u} - \nabla \mathbf{u}^T \cdot \boldsymbol{\tau}_1 \right) = \frac{\eta_1}{\eta_0} \left(\nabla \mathbf{u} + \nabla \mathbf{u}^T \right) \tag{5}$$

where the extra-stress tensor $\boldsymbol{\tau} = \boldsymbol{\tau}_1 + \boldsymbol{\tau}_2$ is splitted into the so-called "particle stress" $\boldsymbol{\tau}_1$ and the "solvent stress" $\boldsymbol{\tau}_2 = 2\eta_2 \boldsymbol{d}$ with the elastic viscosity η_1 and the solvent viscosity η_2; η_0 is the zero shear rate viscosity, λ_1 denotes the relaxation time and $We = \lambda_1 U_0 / L_0$ is the Weissenberg number.

Usual Navier-Stokes boundary conditions are applied for the velocities, i. e. fully developed flow at the flow inlet, no-slip conditions at the rigid walls and traction-free outflow condition. Due to the memory effect of viscoelastic fluids where the state of a fluid particle is determined by its flow history additional boundary conditions have to be set. The results of Renardy [7] show that for Jeffreys' models it is sufficient to prescribe all components of the extra-stress at the inlet boundary.

The numerical solution of the governing equations applies the finite element method. Due to limitations in computer resources the present study uses a decoupled method [5] where the computation of the particle stresses is separated from the solution of the kinematic equations. From known kinematics the viscoelastic particle stresses are calculated. Then the kinematics are updated with the current particle stresses. This procedure is iterated upon corresponding to Picard's iterative scheme.

In this way special numerical techniques for the computation of the extra-stresses that take into account the hyperbolic character of the constitutive equation can be easily used. As the Galerkin approach tends to produce spurious oscillations in the numerical solution a streamline-upwind (SU) scheme is applied in this study.

3 Results & Discussion

3.1 Aortic flow

Numerical results of the velocity patterns and wall shear stress distributions occurring in the ascending aorta are presented. Blood is modeled as Newtonian fluid with a constant density of $\rho = 1050\ kg/m^3$ and the constant viscosity $\mu = 3.65 \cdot 10^{-3}\ Pa\,s$. With the mean inflow diameter used as reference length $L_0 = 2.71 \cdot 10^{-2} m$ and the mean inflow velocity $U_0 = 1.32 \cdot 10^{-1}\ m/s$ the resulting mean Reynolds number is $Re = 1024$ yielding a peak Reynolds number of 4025. The flow rate is about $76 \cdot 10^{-6}\ m^3/s$. The Womersley number is $\alpha = 19.72$ ($\alpha = L_0\sqrt{\omega/\nu}/2$) where $\omega = 7.34\ s^{-1}$ is the angular frequency.

During the systolic phase a significant jet flow occurs in the vessel center while zones of reversed flow can be seen at the walls in the inflow region. Due to high Reynolds number and frequency parameter of the pulsation the development of the boundary layer is restricted to a narrow region on the wall. In the whole vessel segment the velocity profiles are flat and a noticeable skewing to the inner wall can be observed at the entrance of the aortic arch. Flow deceleration causes reversed flow at the walls starting at the inner wall in the arch leading to C-shaped profiles (Figure 1). The comparison between the computational result and the MRI data at cross-section F demonstrates a good qualitative correspondence.

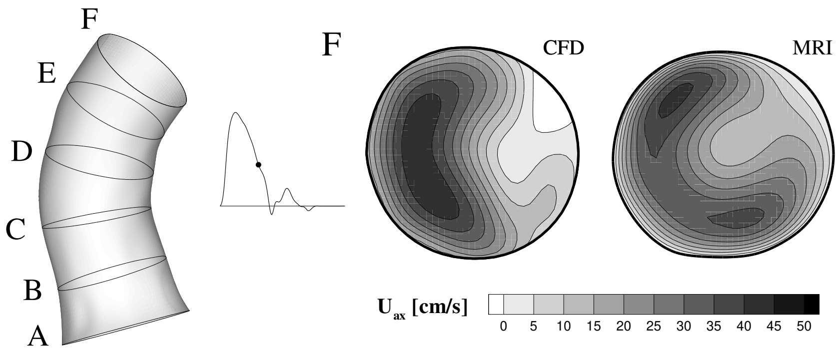

Figure 1: Axial velocity contours at cross-section F during systolic deceleration; comparison between CFD result and MRI measurement.

Wall shear stress distribution during systolic deceleration demonstrates a large zone of recirculation at the inner wall at the beginning of the aortic arch and on the anterior wall (Figure 2). Also the regurgitation at the flow inlet can be observed (indicated with arrows in Figure 2) expressed by negative axial wall shear stresses in the entrance region.

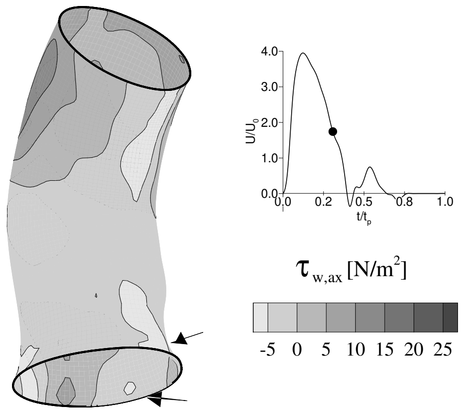

Figure 2: Axial wall shear stress distribution during systolic deceleration (arrows indicate zones of regurgitation at the entrance)

3.2 Viscoelastic flow

Numerical flow simulations have been carried out in three-dimensional 90° curved tubes: a healthy model and a segment with a stenosis of 75% area reduction at the inner wall at the end of the bend. With the centerline radius of the curve $R = 3\,d$, where d is the diameter of the tube, the Dean number is $\kappa = 40.8$ ($\kappa = Re\sqrt{d/2R}$). The inflow and outflow lengths of the tube are $4\,d$ and $15\,d$, respectively. The studies apply the mean velocity $U_0 = 6.15\;cm/s$, the reference length $L_0 = 0.62\;cm$, the Newtonian reference viscosity $\eta_0 = 4.0 \cdot 10^{-3}\;Pa\,s$ and the constant fluid density $\rho = 1050\;kg/m^3$ leading to a Reynolds number $Re = 100$. These parameters represent the Newtonian fluid flow that will serve as a reference. Due to the high shear rates occurring in relatively undisturbed large artery flow red blood cells can hardly form rouleaux [8], and thus the viscoelastic relaxation time $\lambda_1 = 0.03\;s$ corresponds to the characteristic deformation time of a single RBC. The elastic viscosity $\eta_1 = 4.0 \cdot 10^{-4}\;Pa\,s$ and the viscous viscosity $\eta_2 = 3.6 \cdot 10^{-3}\;Pa\,s$ are taken from results by Thurston [9] under the assumption of a representative shear rate of $80\;s^{-1}$. The resulting Weissenberg number is $We = 0.3$.

In Figure 3 the axial velocity profiles of the different fluids are plotted in the plane of symmetry ($z = 0$) for the healthy segment and the stenosed curved tube. The comparison between Newtonian reference fluid (dashed) and Oldroyd-B fluid (solid) are minuscule in case of the healthy configuration. This changes for the disturbed flow in the stenosed tube. The peak velocity of the viscoelastic flow increases downstream the stenotic throat and the shift of the peak velocity towards the outer wall is more pronounced for the viscoelastic fluid. The zone of reversed flow is also slightly enlarged.

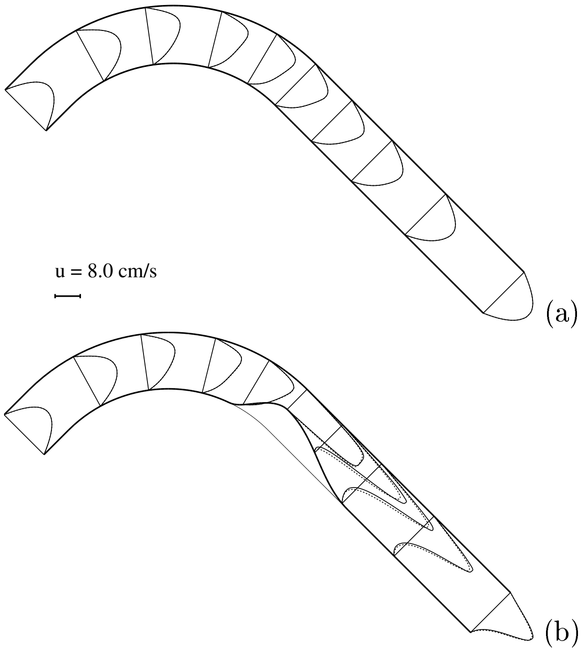

Figure 3: Axial velocity profiles in symmetry plane; ---- Newtonian reference flow: $Re = 100$, —— viscoelastic fluid: $Re = 100$, $We = 0.3$; (a) healthy configuration and (b) stenosed tube

4 Conclusion

The link of CFD and MRI allows more accurate blood flow simulations in moving vessels of complex geometry. These non-invasive techniques constitute an important tool for the understanding of arterial blood flow phenomena in general and the further investigation of hemodynamic related risk factors for arterial disease. The main aspect for further studies will be the investigation of blood flow downstream of artificial aortic valves, the comparison to healthy flow and – as long term objective – to contribute to optimal valve design in humans.

In human blood flow studies in large arteries the viscoelastic effects are usually neglected. This seems to be justified by the fact that in normal physiological blood flow in large vessels the maximum occurring shear rates during the cardiac cycle lie sufficiently above the threshold to break the RBC aggregates. In pathologically altered configurations, however, blood flow may be significantly affected by non-Newtonian properties. This study shows the influence of viscoelastic properties of blood under disturbed flow conditions.

Acknowledgments

This study is supported by the Austrian Science Foundation, Project-No. P 14 321-TEC, Vienna, Austria, and by EUREKA Project No. E!2061.

References

[1] M. Hofer and K. Perktold, Vorkonditionierter konjugierter Gradienten Algorithmus für große schlecht konditionierte unsymmetrische Gleichungssysteme, *Supplement Volume ZAMM Z. angew. Math. Mech.*, 75 SII (1995), 641–642.

[2] T.J.R. Hughes, W.K. Liu, and T.K. Zimmermann, Lagrangian-Eulerian finite element formulation in incompressible viscous flows, *Comp. Methods Appl. Mech. Engrg.* **29**, (1981), 329–349.

[3] G. Karner, K. Perktold, M. Hofer and D. Liepsch, Flow characteristics in an anatomically realistic compliant carotid artery bifurcation model, *Comp. Meth. Biomech. Biomed. Eng.* **2**, (1999), 171–185.

[4] S. Kozerke, *Assessment of heart valve function by motion adapted magnetic resonance imaging*, PhD thesis, Swiss Federal Institute of Technology Zurich, 2000.

[5] A. Leuprecht and K. Perktold, Computer simulation of non-Newtonian effects on blood flow in large arteries, *Comp. Meth. Biomech. Biomed. Eng.* **4**, (2000), 149–163.

[6] J.A. Moore, D.A. Steinman, D.W. Holdsworth and C.R. Ethier, Accuracy of computational hemodynamics in complex arterial geometries reconstructed from magnetic resonance imaging, *Ann. Biomed. Eng.* **27**, (1999), 32–41.

[7] M. Renardy, Recent advance in the mathematical theory of steady flows of viscoelastic fluids, *Journal of Non-Newtonian Fluid Mechanics*, **29**, (1988), 11–24.

[8] M.K. Sharp, G.B. Thurston and J.E. Moore, The effect of blood viscoelasticity on pulsatile flow in stationary and axially moving tubes, *Biorheology*, **33**, (1996), 185–208.

[9] G.B. Thurston, Rheological parameters for the viscosity, viscoelasticity and thixotropy of blood, *Biorheology*, **16**, (1979), 149–162.

E-Mail for K. Perktold: perktold@matd.tu-graz.ac.at

Armin Leuprecht, Institute of Mathematics, Graz University of Technology,
Steyrergasse 30/3, A-8010 Graz, Austria,
Tel.: +43 316 873 8122, Fax: +43 316 873 8621, mail: armin.leuprecht@tugraz.at

Alexander Panfilov
E-Mail: A.V.Panfilov@bio.uu.nl

Dept. of Theoretical Biology
Utrecht University

Electrophysiological model of the heart and its application to studying of cardiac arrhythmias

Abstract

Cardiac arrhythmias are the leading cause of death in the industrialized countries accounting for about 1 death in 10. In most cases, cardiac arrhythmias occur due to abnormalities of propagation of electrical waves of excitation in the heart. This article reviews basic regimes of abnormal wave propagation in cardiac tissue such as reentrant sources or spiral waves and the relation between dynamics of the reentrant source and type of cardiac arrhythmia. We discuss the possible mechanisms of onset of ventricular fibrillation such as the restitution hypothesis, Moe's multiple wavelet hypothesis, the idea of induced fibrillation and spiral breakup. We describe a new approach in mathematical cardiology: the development of a realistic computer model of the heart. This model is based on detailed anatomical data of heart structure and fiber orientation. Finally, we present the results of a study of ventricular fibrillation using an electrophysiological model of the heart. We show the patterns of excitation which occur on the surface and in the interior of the heart discuss the problem of quantification of ventricular fibrillation and possible implications of the restitution hypothesis for pharmacological management of ventricular fibrillation.

1 Propagation of excitation in the heart

The human heart has four chambers: the right and the left atrium and the right and the left ventricle. In normal conditions, the heart is excited approximately once a second. Each excitation initiates a cardiac contraction. The general direction of excitation of the heart is from atria to ventricles (Fig. 1). In normal conditions the excitation of the heart originates in the sino-atrial (S-A) node, which is located in the right atrium.

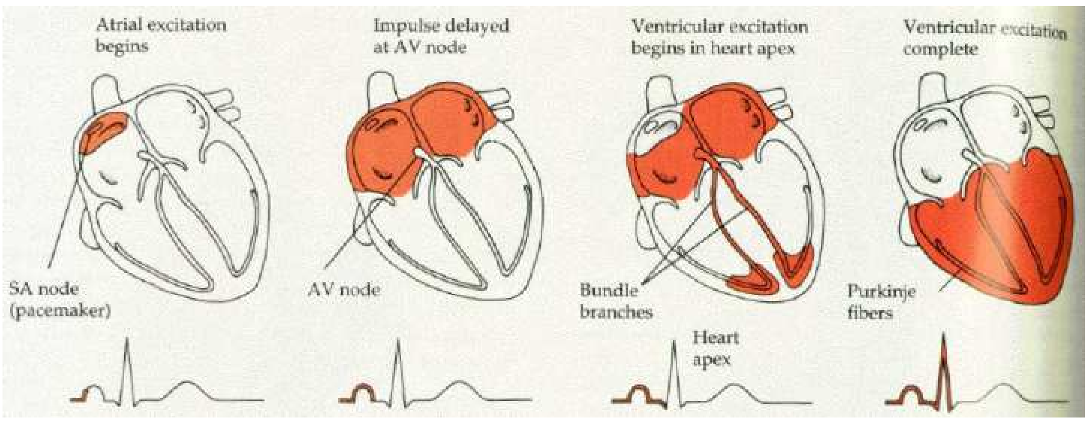

Figure 1: Excitation of the heart (from [Netter, 1989])

The S-A node is a small strip of specialized muscle which is capable of self-excitation. The impulse that originates in the S-A node travels outward in all directions and excites all fibers of the two atria. The velocity of conduction in the atrial muscle is approximately 0.3 meter per second. However, there are many bundles of atrial muscle which conduct the cardiac impulse at a higher velocity. Excitation of the atria is followed by excitation of the ventricles. Almost everywhere the atria are electrically uncoupled from the ventricles. In normal conditions there is only one site where they are connected. The excitation of the ventricles is transmitted from atria at the atrioventricular (A-V) node, which is located in the intra-atrial wall between the atria and the ventricles. Because the propagation through the A-V node is very slow, there is a delay between the atrial excitation and the ventricular excitation. From the A-V node the impulse spreads rapidly through a specialized conducting system to the muscle fibers of the ventricles. The conducting system is formed by the bundle of His, its branches and the Purkinje network. It transmits impulses to the endocardial surface of the left and right ventricle [Durrer et al., 1970]. The propagation velocity of the excitation is at least 1.5 meters per second. Following propagation through the conduction system the excitation enters the ventricular tissue. The excitation propagates from the endocardial surface to the epicardial surface of the ventricles. The velocity of propagation in ventricular myocardium is about 0.5 meter per second, but the ventricular tissue has a complicated rotational anisotropy [Streeter, 1979], so the cardiac impulse does not necessarily travel directly towards the epicardium but may instead angulate along the fibers.

In abnormal conditions, the heart can be excited through the other pathways. Such abnormal propagation of excitation causes many dangerous cardiac arrhythmias.

Generation of a pulse of excitation in the heart, also called an action potential, is a complex process which involves interaction of many inward and outward ionic currents (Fig. 2). The most important of them are, the fast Na^+ inward current, which starts cardiac excitation, the Ca^{2+} inward current and the K^+ outward current, the latter two being responsible for the action potential duration (APD). Detailed description of these currents requires a large system of differential equations [DiFrancesco and Noble, 1985, Luo and Rudy, 1994]. However many important facts can be understood from a simple concept of propagation of excitation, the so called concept of excitable medium.

2 Reentrant sources of excitation in an excitable medium

The general concept of an excitable medium provides a simplified model of cardiac excitation which considers only two properties of cardiac propagation. This medium can conduct pulses of excitation; some time after excitation a *refractory period* sets in, during which a second wave cannot be initiated.

One of the most striking phenomenon in two-dimensional excitable media is the existence of reentrant patterns or spiral waves. If we consider a thin ring of excitable tissue, and initiate a single wave which propagates in one direction, than this wave will make a complete turn during the time (Fig.3).

$$T = l/V, \tag{1}$$

where V is the wave velocity, l length of the ring and T the period of rotation.

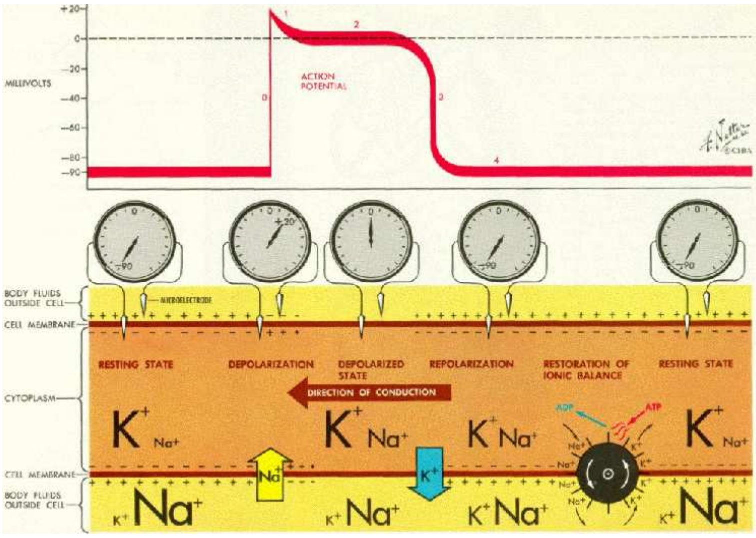

Figure 2: Schematic representation of generation of cardiac action potential (from [Netter, 1989]).

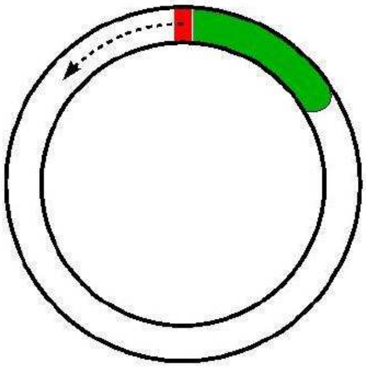

Figure 3: Circulation of excitation in a ring of cardiac tissue

If the time is longer than the refractory period, than this wave will continue to rotate. This sustained rotation of a wave in a ring is an example of one-dimensional reentry [Courtemanche et al., 1993].

Let us consider an extension of this procedure to two dimensions. Assume that we have a 2-dimensional tissue with an inexcitable obstacle. Consider a wave front initially located along a straight line, which starts propagation in one direction. We see (Fig.4 a, b, c) that different points of the front move along different trajectories. The point at the tip of the front rotates around the obstacle, while the point far from the obstacle, moves straight to the right. This results in curving of initially straight wavefront, and formation of a stationary spiral shape (Fig.4d), which will rotate with some period. It turns out that such spiral waves can also exist in excitable media without any inexcitable obstacle. In this case the spiral wave creates this obstacle itself, because of refractory properties of the medium, or because of curvature effects.

Formation of spiral waves in the heart results in the occurrence of cardiac arrhythmias. This is because, as we discussed earlier, in normal conditions the cardiac rhythm

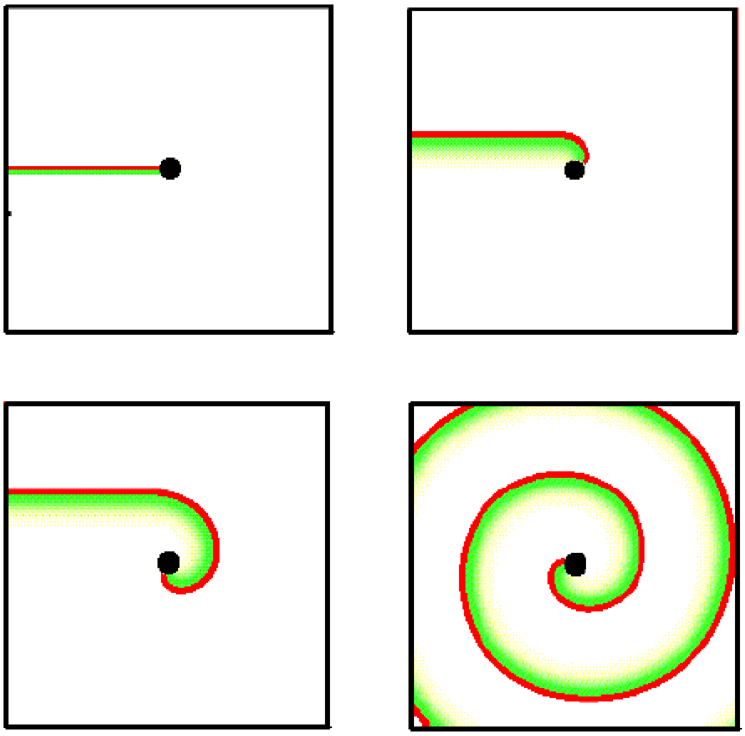

Figure 4: Formation of a spiral wave rotating around an inexcitable obstacle

is determined by the period of a pacemaker (S-A node). The period of a spiral wave is 2 to 3 times shorter than the period of the SA node allowing a spiral wave to suppress the SA node. When this occurs heart starts contracting with the period of the spiral, i.e. 2 to 3 times faster than normal. These faster rhythms are called tachycardias.

The dynamics of the spiral waves rotation determine the type of cardiac arrhythmia observed. Important here is the region close to the center of the spiral usually called the core of the spiral wave. It determines the main properties of this rotating spiral wave [Panfilov and Pertsov, 1981, Winfree, 1990]. The simplest example of a core is circular (Fig.5left). In this case the tip of a spiral wave rotates along a circle. The rotation of the spiral, in this case, is stationary, the period of rotation is constant. Such spiral waves usually occur in excitable media with low excitability, when the curvature effects dominate refractoriness. If the excitability of the medium increases, the rotation becomes non-stationary, and different types of meandering of the spiral occur (Fig. 5): hypocycloid, drift, hypercycloid rotation and finally linear core.

One widely discussed hypothesis connects the dynamics of spiral wave rotation to the type of cardiac arrhythmia [Abildskov and Lux, 1991] and [Gray et al., 1995b]. It is assumed that stationary rotation of a spiral wave corresponds to a periodic ECG (monomorphic tachycardia), different types of non-stationary rotation result in non-periodic ECGs (torsades de pointes, polymorphic tachycardia), and, if a spiral breaks down into a spatio-temporally chaotic pattern in the ventricles of the heart, it results in ventricular fibrillation.

During ventricular fibrillation excitation of the heart is not spatially synchronized. As a result, the heart fails to contract synchronously and fails to pump blood to the

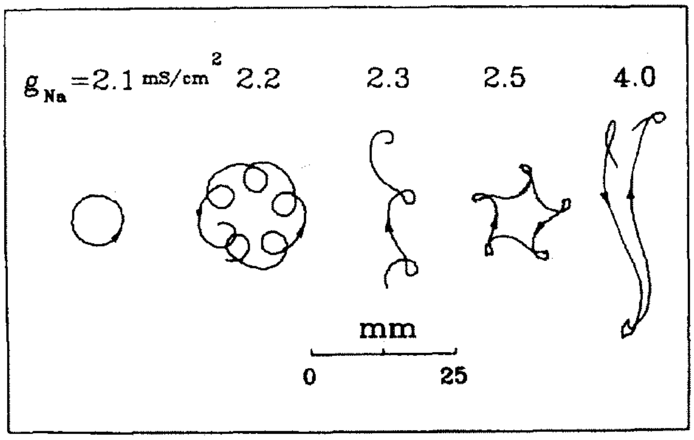

Figure 5: Types of core of spiral wave. The excitability of the medium increases with increase of the model parameter g_{Na}. From [Efimov et al., 1995]

body adequately. This results in sudden cardiac death. Ventricular fibrillation is the main cause of death in the industrialized world [Pool, 1990, Gettes et al., 1995]. The next sections discuss the mechanisms of ventricular fibrillation.

3 Mechanisms of ventricular fibrillation based on heterogeneity of cardiac tissue

3.1 Moe's multiple wavelet hypothesis

For almost four decades now the dominating hypothesis about the mechanism of ventricular fibrillation (VF) has been Moe's multiple wavelet hypothesis [Moe et al., 1964]. Moe constructed the multiple wavelet hypothesis on the basis of computer simulations of a two-dimensional array of coupled excitable elements (cellular automata) with randomly distributed refractory periods. According to Moe, fibrillation occurs as a result of the heterogeneity of cardiac tissue in the refractory period. It is initiated by a train of external stimuli with extremely short coupling intervals of almost the same length as the minimal refractory period of myocardial cells. At such short intervals, cells with refractory periods exceeding the stimulation period do not have enough time to recover and fail to respond. This results in fragmentation of the excitation waves and formation of multiple wavelets. The latter wander randomly through the myocardium forming non-sustained reentry loops. Occasionally, wavelets disappear when they collide with another wavelet or with the boundary. They can also break up, producing daughter wavelets after they encounter refractory cells. Moe's simulations showed that such irregular activity can be self-sustaining if the size of the tissue and the number of wavelets are sufficiently large.

Moe's hypothesis successfully explained experimental phenomena such as the persistence of fibrillation after elimination of the initial triggering and the existence of a critical mass (for a review see [Allessie, 1995]). However, as Moe clearly realized, his hypothesis lacked specific quantitative predictions that could be tested experimentally.

To correct for this deficiency, numerous attempts have been undertaken to characterize the spatial distribution of refractory periods in normal and diseased myocardium, as well as to determine the relationship between this distribution and the incidence of VF (for review see [Janse, 1998, Antzelevitch et al., 1999]). These studies have revealed convincing evidence of a positive correlation between increased heterogeneity in refractory periods and fibrillation. However, these studies suffer from a major technical limitation: the intrinsic complexity of the experimental protocol for measuring the refractory period prevents such measurements from being made at a large number of points. Therefore they do not prove that heterogeneity in refractory periods is indeed a necessary condition for both the initiation and maintenance of VF.

3.2 The single source hypothesis

In an article by [Moe and Abildskov, 1959] another mechanism of fibrillation was proposed. In this mechanism fibrillation is also organized by multiple wavelets, but these wavelets are not sustained but are continually induced by some rather stable, rapid source/sources of excitation located intramurally. Due to the high frequency of the sources, the generated waves break, producing complex activation patterns characteristic of fibrillation. The difference between this mechanism and the previous one is that if one identifies and removes this rapid source, it will stop the fibrillation. Recently the possibility of such fibrillation, also called induced fibrillation or fibrillatory propagation, was considered in relation to atrial fibrillation [Jalife et al., 1998] and has been demonstrated in the human heart. Specifically, it has been shown that a source of atrial fibrillation can be identified and removed by an ablation procedure which terminates the fibrillation [Jais et al., 1997].

Recently, strong experimental evidence has shown that VF, at least in some cases, can also be regarded as "induced" fibrillation. See, e.g., [Zaitsev et al., 2000]. These authors studied the distribution of excitation frequencies on the epicardial and endocardial surfaces during VF. The major finding of this study was that the typical frequency map appeared to be unexpectedly simple and organized. It consisted of few relatively large domains (averaging 1.1 cm^2 in area) with uniform frequency within each domain. These data suggest that high-frequency intramural source drives the fibrillation and that the complex patterns are secondary processes due to the interaction of waves from this source with the heterogeneities of the medium. An extended review of these topics can be found in [Panfilov and Pertsov, 2001].

4 Spiral breakup and restitution hypothesis

Exponential growth in computational power and the increasing availability of computers in recent decades have significantly extended the possibilities for computer modeling of excitation propagation in the heart. Studies of cardiac propagation in cellular automata models have been superseded by studies in so-called ionic models of cardiac tissue which describe in a much more accurate way electrotonic interactions between adjacent cells and transmembrane ionic currents. The first attempts to use such models to simulate functional reentry (also referred to as rotor or spiral wave) in large two-dimensional cell layers led to the following unexpected discovery. Immediately after initiation, a single spiral wave becomes fragmented into a complex pattern of

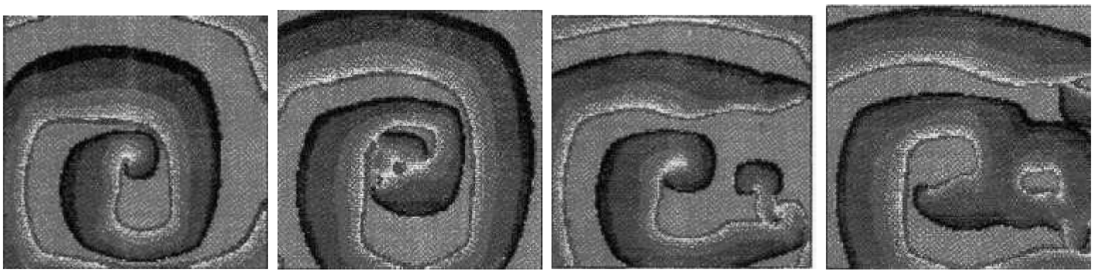

Figure 6: Spiral breakup in a [Noble, 1962] model of cardiac tissue. From [Panfilov and Holden, 1990]. Sequential snapshots of potential distribution a) t=1720 msec, b) t=1880 msec, c) t=2920 msec, d) t=3080 msec. Potentials are coded in equal 10 mV steps, from -85 mV (dark) to +5 mV (white).

activation reminiscent of fibrillation. An example of such a computations is shown in Fig. 6. The computation starts with one rotating spiral wave (Fig. 6a). After several rotations, the spiral wave breaks in the vicinity of the core (Fig. 6b), producing a daughter wavelet. The latter curls, attempting to form another spiral. However, eventually it also breaks, producing further fragmentation and complicating the activation pattern (Fig. 6c). The region of chaotic behavior gradually extends to the whole medium, leading ultimately to a complex pattern that comprises many wavelets of various sizes (Fig. 6d). The dynamics of this process qualitatively reproduces the experimentally observed transition from ventricular tachycardia to VF. This pattern is similar to the fibrillation described by Moe but with one important difference: it occurs in homogeneous cardiac tissue. This phenomenon has been termed "spiral breakup" (the “restitution” hypothesis) and has become the basis for an alternative to Moe’s multiple wavelet hypothesis.

The first computational observation of spiral wave breakup was reported in 1981 [Kuramoto and Koga, 1981] in a model (the so-called $\lambda - \omega$ system) that was different from the models of cardiac tissue. This report remained unnoticed for almost a decade until the phenomenon was rediscovered at the beginning of the 90s in ionic models of cardiac tissue [Winfree, 1989, Panfilov and Holden, 1990, Panfilov and Holden, 1991, Courtemanche and Winfree, 1991] and in cellular automata models of excitable media [Gerhard et al., 1990, Ito and Glass, 1991]. Fig. 7 illustrates spiral breakup in different models. Although the models differ significantly, the main pattern of excitation during breakup is similar in all cases: the wavelets occur as a result of fragmentation of the spiral wave, close to its core.

4.1 A mechanism of spiral breakup

Although the precise mechanism of spiral breakup is still unknown, there is considerable evidence that it is closely connected with the so-called alternans instability. The alternans instability is an instability which occurs if one paces cardiac tissue with a sufficiently high period. In that case, instead of a regular response, the duration of successive action potentials alternate: we usually get short-long-short-long etc. action potentials.

The mechanism of APD alternans is governed by the slope of the APD restitution curve [Nolasco and Dahlen, 1968], [Guevara et al., 1984], and

Figure 7: Patterns of excitation after several rotations of a spiral wave in (a) $\lambda - \omega$ model. Reproduced with permission from [Kuramoto and Koga, 1981], (b) in a cellular automata model (reproduced with permission from [Ito and Glass, 1991]) (c) in a modified FitzHugh-Nagumo model (from [Panfilov and Hogeweg, 1993])

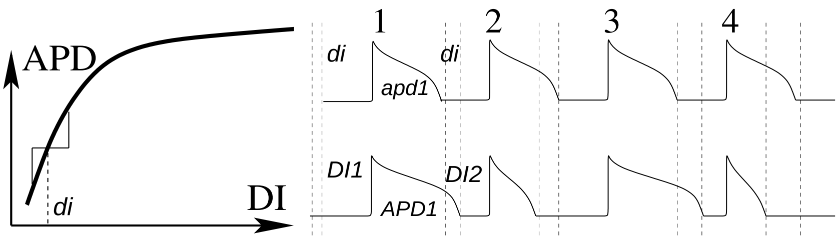

Figure 8: (a) Schematic representation of the APD restitution curve. The thick solid line is the restitution curve, the thin sold line shows deviations of DI and the corresponding deviations of APD around point di. (b) schematic representation of a periodic stimulation (the upper panel) and of the instability growth (the lower panel). Further explanations are in the text.(From [Panfilov and Pertsov, 2001]).

[Courtemanche et al., 1996]. This curve relates the action potential duration to the diastolic interval (DI), which is the time that has elapsed between the end of the preceding action potential and the start of the next one (see Fig. 8a). There is a simple criterion for governing the onset of the alternans: the alternans occur if at the pacing frequency the slope of the restitution curve is greater than one. This criterion can be understood from Fig. 8b which shows the response of cardiac tissue to rapid pacing with a period corresponding to a steep part of the restitution curve (slope is more than one) [Panfilov and Pertsov, 2001]. Because a slope that is more than one means that a small change in di results in a larger change in apd, a small difference between di and $DI1$ (the lower panel) results in larger difference between $apd1$ and $APD1$, which in turn results in a larger difference between di and $DI2$ etc, leading to instability.

4.2 Spiral breakup hypothesis and experiment

Until recently, there was no experimental evidence to support the spiral breakup hypothesis. Data on restitution properties of myocardium indicated that the slopes of the restitution curve were consistently less than one (see e.g. [Elharrar and Surawicz, 1983]). The situation changed dramatically after [Koller et al., 1998] demonstrated steep restitution curves with a maximum slope greater than one in dog myocardium. According to the authors, previous failures to observe such slopes can be attributed partially to the fact that the restitution was measured at quite a long period of stimulation (usually 500 or 300ms). [Koller et al., 1998] developed a new approach (the dynamic restitution protocol) which enabled measurements to be made for short cycle lengths (100-300ms) and during VF.

Additional support for the restitution hypothesis has been obtained from studies by [Riccio et al., 1999, Garfinkel et al., 2000] who demonstrated that certain drugs can flatten the restitution curve and also prevent the occurrence of VF. [Riccio et al., 1999] have shown that *diacetyl monoxime* and *verapamil* significantly reduce the slope of the restitution curve. These drugs not only prevented VF but also converted the existing VF into a regular periodic activity. Similar results were obtained by [Garfinkel et al., 2000] with another drug, *bretylium*. [Garfinkel et al., 2000] mapped also the electrical activity in the tissue. They showed that *bretylium* converts multiple irregular wavelets into stationary spiral waves. [Riccio et al., 1999] found that another anti-arrhythmic drug *procainamide*, which did not reduce the slope of the restitution curve, neither prevented the induction of VF, nor regularized VF. The experiments by [Riccio et al., 1999] also provide a plausible explanation why the breakup mechanism was never observed in early optical mapping studies. These studies utilized *diacetyl monoxime* and *verapamil* as electro-mechanical uncouplers to prevent mechanical artifacts. The fact that these drugs also flatten the restitution curve makes spiral wave breakup less likely.

5 Studying spiral breakup in an anatomical model of the heart

We will start with a description of the model and of the method of computation and later present results on the study and quantification of spiral breakup in the ventricles of the heart.

5.1 Model for the ventricles of heart

In this section we describe our model of the heart which was developed in [Panfilov and Keener, 1993, Panfilov and Keener, 1995]. It is based on the detailed measurements for cardiac anatomy reported in [Nielson et al., 1991, Hunter et al., 1997]. Here we consider the two major parts of this model: the equations for cardiac tissue and the structure of the model. A more detailed description of this model can be found in [Panfilov, 1997].

Model for cardiac tissue. The model in [Panfilov and Keener, 1995] uses FitzHugh-Nagumo equations to describe the excitable tissue. In the first modification the following equations were used

$$\begin{cases} \partial e/\partial t = \partial/\partial x_i d_{ij} \partial e/\partial x_j - f(e) - v \\ \partial v/\partial t = \varepsilon(e)(ke - v) \end{cases} \tag{2}$$

Here e represents the transmembrane potential, v is the recovery variable, and d_{ij}, accounts for the anisotropy of cardiac tissue; $f(e) = C_1 * e$ when $e < e_1$; $f(e) = -C_2 * e + a$ when $e_1 \leq e \leq e_2$; $f(e) = C_3 * (e - 1)$ when $e > e_2$, and $\varepsilon(e) = \varepsilon_1$ when

$e < e_1$; $\varepsilon(e) = \varepsilon_2$ when $e_1 \leq e \leq e_2$; $\varepsilon(e) = \varepsilon_3$ when $e > e_2$. The parameters determining the shape of the function $f(e)$ are $e_1 = 0.0065, e_2 = 0.841, C_1 = 20, C_2 = 3, C_3 = 15, a = 0.15, k = 3$. The function $f(e)$ specifies fast processes such as the upstroke of the action potential. The dynamics of the recovery variable v in (2) is determined by the function $\varepsilon(e)$. In $\varepsilon(e)$ the parameter ε_1 specifies the duration of the refractory tail, and ε_3 specifies the duration of the excited state. Either of these states can be lengthened by decreasing the corresponding value of ε. We used the following values for parameters: ${\varepsilon_1}^{-1} = 1.0$, ${\varepsilon_2}^{-1} = 17.$ and ${\varepsilon_3}^{-1} = 0.1$ These equations represent a realistic model for the propagation of excitation but they give a simplified representation of the ionic transmembrane currents.

Although the model (2) accurately describes the qualitative aspects of excitation propagation, it fails to simulate several quantitative parameters of cardiac tissue such as the shape of the action potential and the restitution properties of the tissue.

The restitution of cardiac tissue shows how the duration of action potential, APD, depends on cycle length, CL [Elharrar and Surawicz, 1983]. In myocardium there is a quite strong dependence: for example, ventricular APD in canine myocardium changes from 330 ms at CL=5000 ms to 150 ms at CL=350 ms [Elharrar and Surawicz, 1983]. Such a shortening of the action potential is very important, especially at the initial moment of formation of cardiac arrhythmia when the heart rate suddenly increases.

In [Aliev and Panfilov, 1996] we proposed a simple model which simulates the restitution property of cardiac tissue, adequately represents the shape of action potential and can be used effectively in computer modeling of the heart. The equations of this model are as follows:

$$\left\{ \begin{array}{rcl} \partial e/\partial t &=& \partial/\partial x_i d_{ij} \partial e/\partial x_j - \; ke(e-a)(e-1) - ev \\ \partial v/\partial t &=& \varepsilon(e,v)(-v - ke(e-a-1)) \end{array} \right. \tag{3}$$

where $\varepsilon(e,v) = \varepsilon_0 + \mu_1 v/(e+\mu_2)$, $k = 8, a = 0.15, \varepsilon_0 = 0.002, \mu_1 = 0.2$and $\mu_2 = 0.3$.

In contrast to the previous model (2) we used the term ev instead of v. This improves the description of the shape of action potential. See, e.g., [Krinsky and Poroticov, 1973, Rogers et al., 1996]. In the model (3) for instance, the left branch of the nullcline $\{e_t = 0\}$ does not enter the region where $e < 0$. This prevents the system from becoming super-repolarized, something which occurs typically in the original FHN model but does not exist in real myocardium. Instead of the linear nullcline of the slow variable in the old model, the new model uses a quadratic term. It also improves the description of the action potential shape and makes it easier to fit the restitution properties of myocardium. The model (3) simulates the restitution property of myocardium with good precision.

The structure of the model. To model the propagation in the heart we need to solve Eqs. (2) or (3), in the domain that represents the geometry of the heart. We also need the values of d_{ij} in this domain. The geometry of the heart in our model is based on the detailed measurements of the anatomy of the ventricles of the canine heart [Nielson et al., 1991, Hunter et al., 1997]. These measurements are presented as a finite element model of the heart anatomy which allows the data on the cardiac anatomy and the fiber orientation field throughout the ventricles of heart to be computed with any desired accuracy. The original model developed by [Nielson et al., 1991, Hunter et al., 1997] uses a prolate spheroidal coordinate system. However for computational reasons the model developed by [Panfilov and Keener, 1995] uses the Cartesian coordinate system. Therefore, we have interpolated the anatomical data to the Cartesian coordinate system. Depending on the problem the spatial resolution was 1mm, 0.7mm, or 0.6mm. The size of the integration grid was from 93x93x93 to 153x153x153 elements. The initial interpolation in the prolate spheroidal coordinate system was made using a program *cmiss* which was kindly provided by Dr. P. Hunter.

Tissue anisotropy is determined by the conductivity tensor d_{ij}. Our model implies that cardiac anisotropy has two principal directions: one along the myocardial fiber ($\vec{\alpha}$) and the other orthogonal to the fiber direction [Panfilov and Keener, 1995]. The conductivity tensor in this case can be found using the following [Leon and Horáček, 1991]:

$$d = D_2 * I + (D_1 - D_2)\vec{\alpha}\vec{\alpha}^T \tag{4}$$

where D_1 and D_2 account for the longitudinal and the transversal wave propagation. The values of the coupling coefficients will be found from the following scaling procedure. The space scale in Eq. (2) is fixed from the anatomical data. The ratio of the coefficients D_1 and D_2 is determined by the anisotropy of the tissue. A typical ratio of the velocity of wave propagation along the fibers to the velocity of propagation across the fibers in canine ventricles is 2:1, which gives D_1/D_2=4. To fix the value of D_1 we need to compare the spatial characteristics of excitation patterns in the heart and in our model. In the model [Panfilov and Keener, 1995] this was done by computing the wavelength of re-entry, and scaling it to the experimental value.

In the following section we describe several results obtained using this model.

5.2 Spiral breakup in an anatomical model of the heart

Fig. 9 shows the development of turbulence in model (2). Just as in 2D and 3D cases, breakup starts with a single scroll wave (Fig. 9a) which after several rotations breaks close to its core (Fig. 9b). In the early stages of breakup (Fig. 9d) the regions with regular propagation can still be identified. Over time the regions with chaotic behavior gradually expand and eventually spread over the whole heart (Fig. 9c). For spiral wave breakup to develop into sustained fibrillation, the size of the heart (as measured from top to bottom) has to be greater than the wavelength of the spiral wave, which in this model is 40 mm [Panfilov, 1999b, Panfilov, 1999a].

We have performed a detailed study of turbulence in the heart in model (3). Fig. 10 shows two typical surface patterns of excitation which occur during fibrillation in our model. The patterns are similar to those observed in recent experimental recordings [Gray et al., 1998, Witkowsky et al., 1998]. A substantial amount of spatial organization is visible on the surface of the heart. The pattern which occurs in the small heart is relatively simple; a "figure-of-eight reentry" and a wavebreak close to the base of the heart. In a large heart the patterns of excitation are not so apparent. Although we can see regions of spatially correlated wave propagation, the sources underlying such waves are not apparent.

The dynamics of excitation resembles the dynamics which has been described in [Gray et al., 1998, Witkowsky et al., 1998]. The dynamics in the small heart is quasi two-dimensional. We can nearly always see rotating and drifting rotors on the surface of the heart. This dynamics is similar to the experimentally recorded dynamics [Gray et al., 1998] and to the dynamics of the initial phase of fibrillation [Witkowsky et al., 1998]. Excitation dynamics in the large heart is three-dimensional

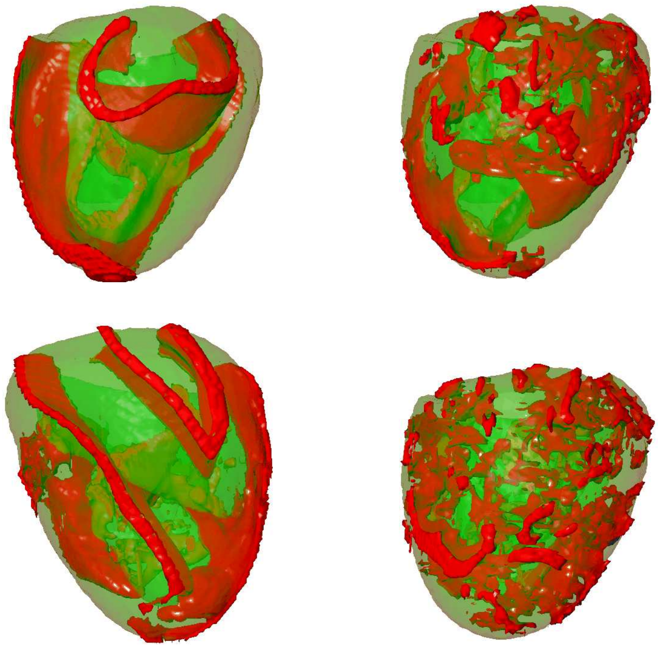

Figure 9: Spiral breakup in an anatomical model of heart. Three-dimensional view of the excitation front is shown at the following times after spiral initiation a) t=500 msec; b) t=1000 msec; c) t=2500 msec d) t=1000 msec (rear view); from [Panfilov, 1997]

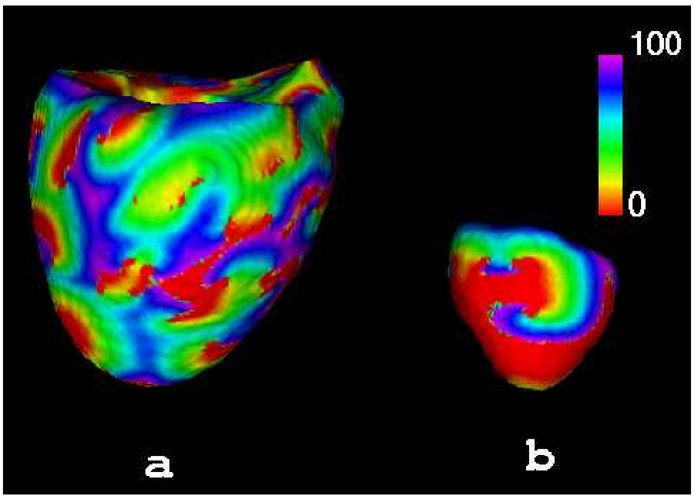

Figure 10: Colored rendering of the activation map on the surface of the heart during ventricular fibrillation due to the process of spiral breakup. Color coding of the activation time in ms is shown by a legend bar. Computations in model (3). The parameters of the model were the following: $a = 0.1, \mu 1 = 0.07; \mu 2 = 0.3, k = 8$. The details about the computational procedure can be found in [Panfilov, 1997]. The tissue anisotropy was 1 : 2 with respect to the velocity of wave propagation. The wavelength of reentry was 40mm. (The wavelength here is the product of the average temporal period during the turbulence and the speed of the wave). a) the size of the heart measured from apex to base is 94mm; b) the size of the heart 48.7mm; (from [Panfilov, 1999a])

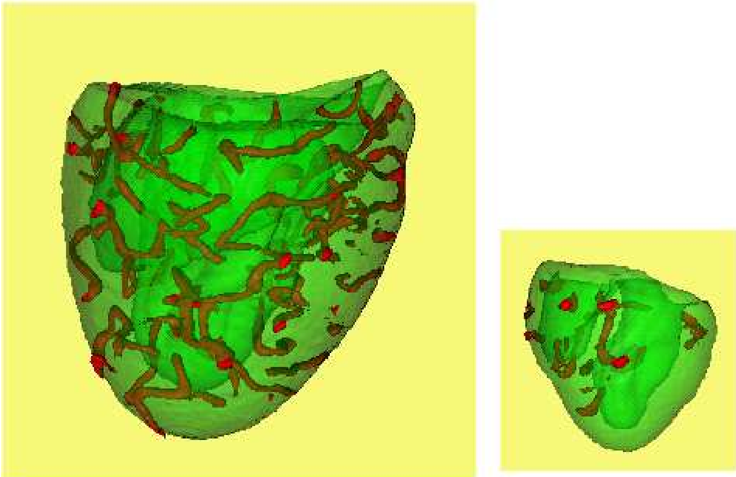

a b

Figure 11: Filaments in the heart during turbulence. a) the size of the heart 94mm; b) the size of the heart 48.7mm; from [Panfilov, 1999a]

and resembles the dynamics of chronic fibrillation [Witkowsky et al., 1998]. There are no persistent rotors on the surface of the heart and usually a considerable amount of excitation comes to the surface from the subsurface mid-myocardial region.

Now let us consider a three-dimensional organization of these wave patterns. The elementary unit of fibrillation in a three-dimensional excitable medium is a line of rotors, or a filament [Winfree and Strogatz, 1984]. Such filaments were found in the BZ reaction [Winfree, 1973, Vinson et al., 1997] as well as in heart, extending from endocardium to epicardium as described in [Frazier et al., 1989]. By means of filaments it is possible to represent patterns of excitation in a three-dimensional excitable medium. Filaments can be regarded as extensions of “phase singularities” on the surface of the heart [Gray et al., 1998]. The use of filaments substantially reduces the amount of information necessary to depict the complex three-dimensional spatio-temporal pattern of fibrillation.

Fig. 11 shows filaments found for patterns of excitation from Fig. 10. We see a large number of filaments (about 50) in the 94mm heart. When the heart is about half that size the number of filaments is substantially less; in fig. 11b we can find only about 10 filaments. If we compare fig. 10b with fig. 11b we see that that “figure-of-eight reentry” is generated by a “U-shaped” filament [Pertsov and Jalife, 1995]. We can also see that the left-upper wavebreak is a part of a short filament extending to the endocardium of the right ventricle. Comparison of fig.10a and fig.11a is much more difficult because there are so many filaments. We can still find a correspondence between the individual filaments and surface dynamics, e.g. several ”figure-of-eight reentries” above the apex of the heart. However, we see that large portions of filaments and even whole filaments are located beneath the surface of the heart. Apparently not all of them are manifested on the surface. These “latent” filaments that cannot be seen on the surface may play an important role in the dynamics of the patterns of excitation because all filaments interact. This can result in complex dynamics [Winfree, 1994b].

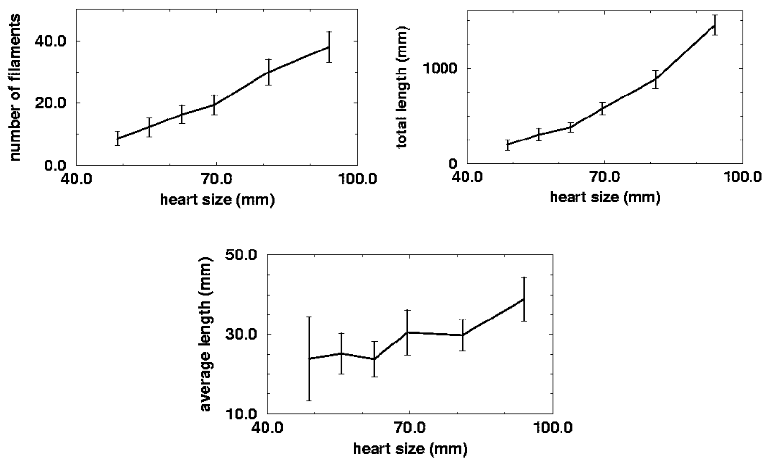

Figure 12: a) number of filaments as a function of heart size (mm), b) total length of all filaments as a function of heart size (mm), and c) the average filament length vs. heart size (mm); (from [Panfilov, 1999a])

Fig. 12 shows the average characteristics of filaments found after analyzing 600 patterns of excitation in the hearts of 7 different sizes. Fig. 12a shows the number of filaments as a function of heart size. For a 94mm heart the average number is 38 ± 4.85, whereas for a 48mm heart the number of filaments is only 8.6 ± 2.30. Thus, the average number of filaments rapidly decreases with decreasing heart size. Fig. 12b shows the total length of all filaments. We see that in a 94mm heart the total length is about 1500mm, which is about 15 times longer than the distance between base and apex. When the size of the heart decreases the total filament length decreases rapidly: in a 48mm heart it is about 200mm, which is only 5 times the heart size. We have also computed the average length of a filament (fig.12c). The average length is found to decrease slightly with decreasing heart size. We also see that there is a large variation in the average filament length, especially in the small heart. In general, the average filament length is of the order of 30mm, which is more than two times larger than the thickness of the thickest myocardial wall of the left ventricle. This together with fig.10a shows that a "regular" filament is not a straight line but is curved. This supports conclusions reported in [Winfree, 1994a], namely that turbulence in the heart becomes persistent if the filament of the rotors can be located transversally to the myocardial walls.

One of the most fundamental properties of ventricular fibrillation is its dependence on the size of the heart. In 1914, Garrey showed [Garrey, 1914] that there is a minimal amount (mass) of tissue necessary to maintain fibrillation. According to Gray et al., [Gray et al., 1995a, Gray et al., 1998], in small hearts (e.g. rabbit) there is usually a simple pattern of excitation, whereas while in large hearts the number of rotors increases and the pattern becomes more complex. To understand better the dependence of ventricular fibrillation on heart size we performed a dimensional analysis of the turbulence in the heart. The main idea of this analysis was to induce the same type of electrical turbulence in hearts of different sizes and to find how the main properties of the turbulence scaled with the geometrical characteristics of the medium, e.g. heart size.

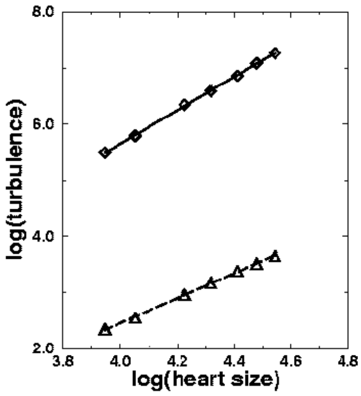

Figure 13: Scaling of ventricular turbulence. The *log* of the total length is shown by the solid line; the *log* of the number of filaments is shown by the dashed line. (from [Panfilov, 1999a])

To characterize the turbulence we used two criteria: the total number of filaments in the heart at a given moment in time and the total length of all filaments comprising the turbulence. The results of such scaling are shown in fig.13. The solid line in fig.13 show estimates for the *log* of the average total length of all filaments during the turbulence vs. *log* of the heart size. We see that the points can be approximated satisfactorily by a straight line. The slope of this line is 2.98 ± 0.025. The dashed line in Fig. 13 shows the *log* of the average number of filaments during the turbulence vs. *log* of the heart size. The slope of this line is 2.15 ± 0.034.

The results of this scaling can be interpreted as follows. The slope 2.98 ± 0.025 indicates that the turbulence in the heart is indeed three-dimensional: the total length of all filaments increases with the volume of the heart in such a way that the filament length per unit volume remains constant. However, is this the correct scaling for the complexity of turbulence in the heart? In our view it is not.

Let us first try to define complexity. As we mentioned above, the total pattern of excitation during turbulence includes many regions each of which is driven by a single filament in three dimensions, or by a spiral in two dimensions. Therefore the complexity of the total pattern can be evaluated as the total number of such regions, i.e. the total number of filaments during the turbulence. Therefore, the first scaling for the complexity is 2.15 ± 0.034 (Fig. 13, long dashed line). The other measure of turbulence used in this paper is the total length of all filaments comprising the pattern. In our view this measure does not properly represent the complexity of fibrillation. Indeed, if we induce a scroll wave at the same location in hearts of different sizes, we find that the length of filament representing this scroll will change with changing heart size. However, the complexity of the pattern of excitation should remain the same. To measure complexity we can use the relative length of the filament with respect to the heart size, instead of the absolute length of a filament. For this purpose we simply divide the length of a filament by the heart size. In such relative units one scroll wave at the same location will have the same length of filament in hearts of all sizes. Such a definition of complexity in relative units reflects the fact that the relatively longer filaments produce more complex patterns of excitation than the short ones. This "definition" of complexity is similar to an experimental procedure in which in order to compare the patterns of excitation in hearts of different sizes we first scale, on a computer screen, hearts to the same standard size and only then compare the patterns of excitation.

Scaling for the *log* of the relative total filament length with the *log* of the heart size will give a slope which is one unit less than the slope in fig.13 for the absolute total filament length. Therefore, the scaling for the complexity using this measure will be 1.98 ± 0.025. We see that the two slopes which we found for the complexity of the turbulence (2.15 ± 0.034 and 1.98 ± 0.025) are reasonably close to each other. This shows that in our definition the complexity dimension of the turbulence in the heart is about 2.

6 Concluding remarks

In this article, we have discussed several applications of the theory of spiral waves in excitable media to important problems of mathematical cardiology. We have also given a brief description of our approach to modeling wave propagation in an anatomical model of the heart. The main focus of the last part of our paper was on modeling ventricular fibrillation via the phenomenon of spiral breakup (the restitution hypothesis). The restitution hypothesis, if proven, provides a new paradigm for screening new anti-arrhythmic drugs, based on measurements of the slope of the restitution curve. Recent major failures of clinical antifibrillatory drug tests have revealed the need for new screening principles. The restitution hypothesis is a good candidate.

Acknowledgments: I am grateful to Dr. E. Cytrynbaum for making valuable comments on this manuscript.

References

[Abildskov and Lux, 1991] Abildskov, J. A. and Lux, R. L. (1991). The mechanism of simulated torsade de pointes in a computer model of propagated excitation. *J. Cardiovasc. Electrophysiol*, 2:224–237.

[Aliev and Panfilov, 1996] Aliev, R. R. and Panfilov, A. V. (1996). A simple two-variable model of cardiac excitation. *Chaos, Solitons and Fractals*, 7:293–301.

[Allessie, 1995] Allessie, M. A. (1995). Reentrant mechanisms underlying atrial fibrillation. In Zipes, D. P. and Jalife, J., editors, *Cardiac electrophysiology. From cell to bedside, 2nd edition*, pages 562–566, Philadelphia. Saunders.

[Antzelevitch et al., 1999] Antzelevitch, C., Yan, G., Shimizu, W., and A., B. (1999). Electrical heterogeneity, the ECG, and cardiac arrhythmias. In Zipes, D. P. and Jalife, J., editors, *Cardiac electrophysiology. From cell to bedside, 3rd edition*, pages 222–238, Philadelphia. Saunders.

[Courtemanche et al., 1993] Courtemanche, M., Glass, L., and Keener, J. P. (1993). Instabilities of a propagating pulse in a ring of excitable media. *Phys. Rev. Lett.*, 70:2182–2185.

[Courtemanche et al., 1996] Courtemanche, M., Keener, J. P., and Glass, L. (1996). A delay equation representation of pulse circulation on a ring of excitable media. *SIAM J. Appl. Math.*, 56:119–142.

[Courtemanche and Winfree, 1991] Courtemanche, M. and Winfree, A. T. (1991). Reentrant rotating waves in a Beeler-Reuter based model of two-dimensional cardiac activity. *Int. J. Bif. and Chaos*, 1:431–444.

[DiFrancesco and Noble, 1985] DiFrancesco, D. and Noble, D. (1985). A model of cardiac electrical activity incorporating ionic pumps and concentration changes. *Phil. Trans. R. Soc. B*, 307:353–398.

[Durrer et al., 1970] Durrer, D., Van Dam, R. T., Freud, G. E., Janse, M. J., Meijler, F. L., and Arzbaecher, R. C. (1970). Total excitation of the isolated human heart. *Circulation*, 41:899–912.

[Efimov et al., 1995] Efimov, I., Krinsky, V. I., and Jalife, J. (1995). Dynamics of rotating vortices in the Beeler-Reuter model of cardiac tissue. *Chaos, Solitons and Fractals*, 5:513–526.

[Elharrar and Surawicz, 1983] Elharrar, V. and Surawicz, B. (1983). Cycle length effect on restitution of action potential duration in dog cardiac fibers. *Am. J. Physiol.*, 244:H782–H792.

[Frazier et al., 1989] Frazier, D. W., Wolf, P. D., Wharton, J. M. Tang, A. S. L., Smith, W. M., and Ideker, R. E. (1989). Stimulus-induced critical points: Mechanism for electrical induction of reentry in normal canine myocardium. *J. Clin. Invest.*, 83:1039–1052.

[Garfinkel et al., 2000] Garfinkel, A., Kim, Y., Voroshilovsky, O., Qu, Z., Kil, J., Lee, M., Karagueuzian, H., Weiss, J., and Chen, P. (2000). Preventing ventricular fibrillation by flattening cardiac restitution. *Proc. Natl. Acad. Sci. USA*, 97:6061–6066.

[Garrey, 1914] Garrey, W. E. (1914). The nature of fibrillatory contraction of the heart, its relation to tissue mass and form. *Am. J. Physiol.*, 33:397.

[Gerhard et al., 1990] Gerhard, M., Schuster, H., and Tyson, J. J. (1990). A cellular automaton model of excitable media including curvature and dispersion. *Science*, 247:1563–1566.

[Gettes et al., 1995] Gettes, L. S., Cascio, W. E., and Sanders, W. E. (1995). Mechanisms of sudden cardiac death. In Zipes, D. P. and Jalife, J., editors, *Cardiac electrophysiology. From cell to bedside, 2nd edition*, pages 527–538, Philadelphia. Saunders.

[Gray et al., 1995a] Gray, R. A., Jalife, J., Panfilov, A., Baxter, W. T., Cabo, C., Davidenko, J. M., and Pertsov, A. M. (1995a). Mechanisms of cardiac fibrillation. *Science*, 270:1222–1223.

[Gray et al., 1995b] Gray, R. A., Jalife, J., Panfilov, A., Baxter, W. T., Cabo, C., and Pertsov, A. M. (1995b). Non-stationary vortex-like reentrant activity as a mechanism of polymorphic ventricular tachycardia in the isolated rabbit heart. *Circulation*, 91:2454–2469.

[Gray et al., 1998] Gray, R. A., Pertsov, A. M., and Jalife, J. (1998). Spatial and temporal organization during cardiac fibrillation. *Nature*, 392:75–78.

[Guevara et al., 1984] Guevara, M., Ward, A., Shrier, A., and Glass, L. (1984). Electrical alternans and period doubling bifurcations. *IEEE Comp. Cardiol.*, 562:167–170.

[Hunter et al., 1997] Hunter, P. J., Smail, B. H., Nielson, P. M. F., and LeGrice, I. J. (1997). A mathematical model of cardiac anatomy. In Panfilov, A. V. and Holden, A. V., editors, *Computational Biology of the Heart*, pages 171–215, Chichester. Wiley.

[Ito and Glass, 1991] Ito, H. and Glass, L. (1991). Spiral breakup in a new model of discrete excitable media. *Phys. Rev. Lett.*, 66:671–674.

[Jais et al., 1997] Jais, P., Haissaguerre, M., Shah, D. C., Chouairi, S., Gencel, L., Hocini, M., and Clementy, J. (1997). A focal source of atrial fibrillation treated by discrete radiofrequency ablation. *Circulation*, 95:572–576.

[Jalife et al., 1998] Jalife, J., Berenfeld, O., Skanes, A., and Mandapati, R. (1998). Mechanisms of atrial fibrillation: mother rotors or multiple daughter wavelets, or both? *J Cardiovasc Electrophysiol*, 9:S1–S12.

[Janse, 1998] Janse, M. J. (1998). Vulnerability to ventricular fibrillation. *Chaos*, 8:149–156.

[Koller et al., 1998] Koller, M., Riccio, M., and Gilmour Jr, R. (1998). Dynamics restitution of action potential duration during electrical alternans and ventricular fibrillation. *Am.J.Physiol*, 275:H1635–H1642.

[Krinsky and Poroticov, 1973] Krinsky, V. I. and Poroticov, V. I. (1973). Method for analysis of drug action on muscle and nerve membranes from voltage clamp data (nullclines method). *Studia Biophys.*, 39(2):69–80.

[Kuramoto and Koga, 1981] Kuramoto, K. and Koga, S. (1981). Turbulized rotating chemical waves. *Prog. Theor. Phys.*, 66:1081–1085.

[Leon and Horáček, 1991] Leon, L. J. and Horáček, B. M. (1991). Computer model of excitation and recovery in the anisotropic myocardium. I. rectangular and cubic arrays of excitable elements. *J. Electrocardiol.*, 24:1–16.

[Luo and Rudy, 1994] Luo, C. and Rudy, Y. (1994). A dynamic model of the cardiac ventricular action potential. I. Simulations of ionic currents and concentration changes. *Circ. Res.*, 74:1071–1096.

[Moe and Abildskov, 1959] Moe, G. K. and Abildskov, J. A. (1959). Atrial fibrillation as a self-sustained arrhythmia independent of focal discharge. *Am. Heart J.*, 58:59–70.

[Moe et al., 1964] Moe, G. K., Rheinbolt, W. C., and Abildskov, J. A. (1964). A computer model of atrial fibrillation. *Am. Heart J.*, 67:200–220.

[Netter, 1989] Netter, F. (1989). *Atlas Of Human Anatomy.* Rittenhouse Book Distributors Inc.

[Nielson et al., 1991] Nielson, P. M. F., LeGrice, I. J., Smail, B. H., and Hunter, P. J. (1991). A mathematical model of the geometry and fibrous structure of the heart. *Am. J. Physiol.*, 260:H1365–H1378.

[Noble, 1962] Noble, D. (1962). A modification of the Hodgkin−Huxley equation applicable to Purkinje fiber action and pacemaker potential. *J. Physiol.*, 160:317–352.

[Nolasco and Dahlen, 1968] Nolasco, J. and Dahlen, R. (1968). A graphic method for the study of alternation in cardiac action potentials. *J. Appl. Physiol.*, 25:191–196.

[Panfilov, 1997] Panfilov, A. V. (1997). Modeling of reentrant patterns in an anatomical model of the heart. In Panfilov, A. V. and Holden, A. V., editors, *Computational Biology of the Heart*, pages 259–276, Chichester. Wiley.

[Panfilov, 1999a] Panfilov, A. V. (1999a). Three-dimensional organization of electrical turbulence in the heart. *Phys. Rev. E*, 59:R6251–R6254.

[Panfilov, 1999b] Panfilov, A. V. (1999b). Three-dimensional wave propagation in mathematical models of ventricular fibrillation. In Zipes, D. P. and Jalife, J., editors, *Cardiac electrophysiology. From cell to bedside, 3rd edition*, pages 271–277, Philadelphia. Saunders.

[Panfilov and Hogeweg, 1993] Panfilov, A. V. and Hogeweg, P. (1993). Spiral break-up in a modified FitzHugh−Nagumo model. *Phys. Lett. A*, 176:295–299.

[Panfilov and Holden, 1990] Panfilov, A. V. and Holden, A. V. (1990). Self-generation of turbulent vortices in a two-dimensional model of cardiac tissue. *Phys. Lett. A*, 147:463–466.

[Panfilov and Holden, 1991] Panfilov, A. V. and Holden, A. V. (1991). Spatio−temporal irregularity in a two-dimensional model of cardiac tissue. *Int. J. Bif. and Chaos*, 1:119–129.

[Panfilov and Keener, 1993] Panfilov, A. V. and Keener, J. P. (1993). Modeling reentry in a finite element model of the heart. *J. Physiol.*, 467:152P.

[Panfilov and Keener, 1995] Panfilov, A. V. and Keener, J. P. (1995). Re-entry in an anatomical model of the heart. *Chaos, Solitons and Fractals*, 5:681–689.

[Panfilov and Pertsov, 1981] Panfilov, A. V. and Pertsov, A. M. (1981). Spiral waves in active media: reverberator in the FitzHugh-Nagumo model. In *Autowave Processes in systems with diffusion*, pages 77–84, Gorky. Acad. Sci. USSR. in Russian.

[Panfilov and Pertsov, 2001] Panfilov, A. V. and Pertsov, A. M. (2001). Ventricular fibrillation: evolution of the multiple wavelet hypothesis. *Phil.Trans.R.Soc.Lond.A.*, 359:1315–1325.

[Pertsov and Jalife, 1995] Pertsov, A. M. and Jalife, J. (1995). Three dimensional vortex-like reentry. In Zipes, D. P. and Jalife, J., editors, *Cardiac electrophysiology. From cell to bedside, 2nd edition*, pages 403–410, Philadelphia. Saunders.

[Pool, 1990] Pool, R. (1990). Heart like a wheels. *Science*, 247:1294–1295.

[Riccio et al., 1999] Riccio, M., Koller, M., and Gilmour Jr, R. (1999). Electrical restitution and spatiotemporal organization during ventricular fibrillation. *Circ Res*, 84:955–963.

[Rogers et al., 1996] Rogers, J., Courtemanche, M., and McCulloch, A. (1996). Finite element methods for modeling impulse propagation in the heart. In Panfilov, A. V. and Holden, A. V., editors, *Computational Biology of the Heart*, pages 217–234, Chichester. Wiley.

[Streeter, 1979] Streeter, D. D. J. (1979). Gross morphology and fiber geometry of the heart. In *Handbook of physiology. - Section 2: The cardiovascular system, Volume I: The heart*, pages 61–112, Bethesda, MD. Am. Physiol. Soc.

[Vinson et al., 1997] Vinson, M., Mironov, S., and Pertsov, A. M. (1997). Control of spatial orientation and lifetime of scroll rings in excitable media. *Nature*, 386:477–480.

[Winfree, 1973] Winfree, A. T. (1973). Scroll-shaped waves of chemical activity in three dimensions. *Science*, 181:937–939.

[Winfree, 1989] Winfree, A. T. (1989). Electrical instability in cardiac muscle: Phase singularities and rotors. *J.Theor. Biol.*, 138:353–405.

[Winfree, 1990] Winfree, A. T. (1990). Varieties of spiral wave behavior: An experimental approach to the theory of excitable media. *Chaos*, 1:303–334.

[Winfree, 1994a] Winfree, A. T. (1994a). Electrical turbulence in three-dimensional heart muscle. *Science*, 266:1003–1006.

[Winfree, 1994b] Winfree, A. T. (1994b). Persistent tangled vortex rings in generic excitable media. *Nature*, 371:233–236.

[Winfree and Strogatz, 1984] Winfree, A. T. and Strogatz, S. H. (1984). Organizing centers for three-dimensional chemical waves. *Nature*, 311:611–615.

[Witkowsky et al., 1998] Witkowsky, F. X., Leon, L. J., Penkoske, P. A., Giles, W. R., Spano, M. L., Ditto, W. L., and Winfree, A. T. (1998). Spatiotemporal evolution of ventricular fibrillation. *Nature*, 392:78–82.

[Zaitsev et al., 2000] Zaitsev, A., Berenfeld, O., Mironov, S., Jalife, J., and Pertsov, A. (2000). Distribution of excitation frequencies on the epicardial and endocardial surfaces of fibrillating ventricular wall of the sheep heart. *Circ.Res.*, 86:408–417.

Michael Rosenblum
E-Mail: MRos@agnld.uni-potsdam.de

Nonlinear Dynamics Group
Dept. of Physics
University of Potsdam

Quantitative analysis of cardiorespiratory interaction in healthy infants

We use the recent developments in the theory of synchronization of irregular (noisy or chaotic) oscillators to address the cardiorespiratory interaction. We discuss the notion of phase for complex systems as well as the methods of instantaneous phase estimation from data. Next, we discuss how the strength of the interaction can be quantified by means of the analysis of interrelation between the phases. We introduce and compare several synchronization indices. Using model and real data sets as examples, we demonstrate that the index based on the stroboscopic approach is mostly suitable for the analysis of cardiorespiratory interaction.

As the next step, we consider the problem of detecting the direction of interaction of two systems. The main idea here is that in case of unidirectional coupling ($1 \to 2$) the perturbations in the system 1 can be traced in the system 2, but not vice versa. We use this idea to introduce the directionality index that quantifies the asymmetry in coupling.

Finally, we report the results of experimental study in a group of healthy infants. We conclude that one of the quantitative measures - the conditional probability index - allows reliable detection of synchronous epochs of different order $n : m$ and, thus, makes possible an automatic processing of large data sets. It turned out that the average degree of synchronization varies with the age of the newborns. The direction of coupling changes as well: the interaction is nearly symmetrical in the first days of life and tends to unidirectional (from respiration to heartbeat) with the maturation.

References

1. R. Mrowka, A. Patzak, and M.G. Rosenblum, "Quantitative analysis of cardiorespiratory synchronization in infants", *Int. J. of Bifurcation and Chaos*, **10**(11), pp. 2479-2488 (2000).
2. A. Pikovsky, M. Rosenblum, and J. Kurths, *Synchronization. A Universal Concept in Nonlinear Sciences*, Cambridge University Press, 2001.
3. M.G. Rosenblum et al., "Phase synchronization: from theory to data analysis", In: *Handbook of Biological Physics*, Elsevier Science, Vol. 4, *Neuro-informatics*, Eds: F. Moss and S. Gielen, Chapter 9, pp. 279-321, 2001.
4. M. Rosenblum and A. Pikovsky, "Detecting direction of coupling in interacting oscillators", *Phys. Rev. E*, **64**, 045202 (2001).

Loring Rowell

Dept. of Physiology and Biophysics
University of Washington School of Medicine

Crucial problems in cardiovascular control during exercise

The two classes of problems discussed are, first, those factors that may enhance or impede optimal mechanical coupling of the heart and vasculature; the second concerns those reflexes thought to control the circulation during exercise.

During much of the 20th century physiologists battled over the importance of the Frank-Starling relationship in control of stroke volume (SV) and cardiac output (CO). They disagreed over the importance of (a) neural control of the peripheral circulation, (b) venomotor control and (c) the muscle pump.

Some major stumbling blocks led to these disagreements. A key one was the large effect of posture on the distribution of blood volume and the ventricular end diastolic volume (EDV) and SV in humans as opposed to negligible effects in quadrupeds. Thus length-tension effects on SV were large in humans (up to a point) and negligible in dogs for example.

A crucial problem was the failure to appreciate the role of physical properties of the various vasculature beds and that the distribution of blood flow among them is a primary determinant of cardiac performance. In his simple model Krogh in 1912 divided the peripheral circulation into compliant and non-compliant regions and proposed that the volume of blood available to fill the heart depended on the fraction of CO directed to compliant regions whose volume expands with increased blood flow.

Early attempts to raise CO by drugs, and later by electrical pacing reveal a limited ability to raise CO owing to coincident decline in central venous pressure (CVP), SV and EDV. The negative slope of the line relating CVP to CO (the independent variable) is due to resistive and capacitive properties of the peripheral vasculature, and was a major feature in Guyton's analysis of "Venous Return" curves (but with independent and dependent variables reversed), later called by Levy (1976) "Vascular Function" curves (with CO as the independent variable). A paradox is that raising CO at rest reduces EDV and SV - yet, maintained or increased EDV and SV are required if CO is to rise normally during exercise.

A recent key experiment was to raise and lower CO by left ventricular pacing in atrioventricular (A-V) blocked dogs during rest and voluntary exercise at different intensities. The slope relating CVP to the normal rise in CO during exercise (normal heart rate by A-V linked pacing) was positive (e.g. as in Guyton's Ventricular Function Curves). But when CO was raised or lowered by ventricular pacing at any given exercise intensity the slopes relating CVP to CO were negative and had the same slope as at rest. Also the slope of the relationship at rest or exercise, was unaffected by autonomic blockade.

The explanation lies in the fraction of CO passively distributed to compliant vs non-compliant regions when CO was increased by pacing alone vs when it was being increased by raising exercise intensity. The ability to raise CO during exercise depends on the distribution of blood flow plus a simultaneous event in the peripheral circulation that translocates vascular volume back to the heart (i.e. the muscle pump).

The importance of flow distribution is most obvious in humans when heat stress during exercise raises skin blood flow (a very compliant circuit). The consequent decline in CVP and SV limits the rise in CO which ultimately levels off (despite rising demand) as CVP approaches zero and central veins reach their collapse point.

The positive relationship between CVP and CO in response to exercise also depends on effective muscle pumping. The muscle pump is a true flow-generating pump whose output must match left ventricular output in order to maintain thoracic blood volume and arterial pressure. At the onset of exercise muscle pumping withdraws volume from arteries thus transiently lowering arterial pressure; it raises muscle blood flow and central venous volume as CO rises and *before peripheral vascular resistance falls.* Because muscle is a true pump calculation of a "virtual" vascular conductance during exercise lacks meaning. In fact muscle can still pump effectively when its perfusion pressure is reduced to zero.

An important unsolved problem is how cardiac performance is affected by mechanical interaction between heart and pericardium and by their interaction with lungs, chest wall and diaphragm that can influence cardiac pumping by altering ventricular transmural pressures. Cutting the pericardium affords the same advantages to the exercising animal as months of physical conditioning by permitting large increments in maximal values of SV and CO and VO_2. This evidence plus the progressive marked rise in pulmonary wedge pressure (PWP) and right atrial pressure at a time when EDV and SV are invariant suggests that a pericardial constraint exists even during submaximal exercise. A probable cause is that exercise-induced increments in cardiac volume raise pericardial volume to the steep portion of the pericardial pressure-volume relationship, which prevents further rise in EDV and SV.

The second class of problems discussed are those concerning what reflexes might control the circulation during exercise. In general we accept that centrally generated neural command signals (or central command) set the basic patterns of effector activity which in turn is modified by *arterial baroreflexes* and reflexes from chemosensitive afferents, called *chemoreflexes*, and mechanosensitive afferents called *mechanoreflexes* in muscle.

Central command acts immediately to raise heart rate (HR) and CO by vagal withdrawal whereas the much slower responding sympathetic responses are initiated later by reflexes. We consider only muscle chemoreflexes (MCR) and arterial baroreflexes; the role of muscle mechanoreflexes is unknown.

Are MCR important tonic controllers of the circulation during exercise; that is does the sympathetic nervous system continuously correct mismatches between blood flow and metabolism? These are FLOW ERRORS causing accumulation of metabolites in muscle or a metabolic error signal that is corrected by increased flow.

Stimulus response curves for the MCR reveal the reflex is not tonically active during mild or moderate exercise because normal blood flow is well above a threshold for the reflex, thus giving a large margin for flow error. In heavier exercise, normal blood flow may be at the threshold for the reflex - we are not sure - but in both cases ischemia and lack of O_2 are required to elicit the reflex, thus weakening the idea of any tonic control.

Are arterial baroreflexes important tonic controllers of the circulation during exercise; that is, does the sympathetic nervous system correct mismatches between CO and vascular conductance or PRESSURE ERRORS?

It is now clear (there is a long history of controversy) that baroreflex sensitivity is unchanged from rest up to severe exercise. It is also true that exercise raises blood pressure together with HR and CO. So where is the error signal? In theory it is the difference between the prevailing pressure and the operating point of the baroreflex which is presumably shifted ("reset") to a higher pressure during exercise.

The cornerstone for the argument for tonic baroreflex control is the recent observation that blood pressure cannot be maintained during exercise without tonic vasoconstriction of active muscle. This is because the ability of skeletal muscle to vasodilate, even in submaximal exercise, can outstrip the pumping capacity of the heart.

Evidence consistent with "resetting" of the reflex is as follows:

1. A functioning arterial baroreflex is essential for the rise in blood pressure with exercise.
2. The baroreflex is needed to raise sympathetic activity and to initiate and maintain regional vasoconstriction during exercise.
3. Suppressing the normal rise in blood pressure with exercise drives sympathetic activity upward to extreme levels - i.e. as though a failure to raise pressure were "perceived" as hypotension by the central nervous system.
4. Stimulus response curves for the carotid sinus reflex reveal that these curves shift progressively to the right and upward to higher and higher operating points (pressures) from rest to mild up to severe exercise.

What provides the stimulus for "resetting" the baroreflex? One theory is that central command, a feed forward controller, can also initiate feedback control by changing the operating point of a reflex, e.g. the baroreflex. This is unproven, but clearly, central command neither raises nor controls blood pressure or sympathetic activity when the baroreflex is inactivated.

Aneta Stefanovska and Maja Bračič Lotrič
E-Mail: aneta@osc.fe.uni-lj.si

Nonlinear Dynamics and Synergetics
Faculty of Electrical Engineering, University of Ljubljana
Tržaška 25, 1000 Ljubljana, Slovenia

Cardiovascular dynamics - Analysis of its oscillations and their synchronization

Abstract. We discuss the experimental evidences indicating that the flow of blood through the cardiovascular system is characterised by oscillatory processes. In cardiovascular signals measured in relaxed healthy subjects, five characteristic frequencies can be identified within the frequency range from 0.0095–1.6 Hz. Each oscillator is coupled with each of the others thus mutually influencing all their frequencies and amplitudes. Control of the cardiovascular system appears to be maintained by a fine balance between the eigenfrequencies of the oscillators, resulting in an interplay between instantaneous amplitude and frequency modulation and synchronization between their phases.

Introduction. Following the pioneering work of Penaz *et al.* [4], Sayers [5] and Akselrod *et al.* [6], a range of spectral analysis techniques have been applied to blood pressure and heart rate variability data, and rhythmic phenomena in these signals have been reported by several authors ([7] and the references therein). Periodic components have also been observed in peripheral blood flow signals measured by laser Doppler flowmetry [8]–[10].

Using the continuous wavelet transfrom to facilitare good low frequency resolution, spectral peaks near 0.1 Hz and below 0.05 Hz – including a frequency component of $\sim$0.01 Hz – were revealed in several simultaneously measured signals [11], in addition to the more obvious respiratory and cardiac oscillations. The questions therefore arise as to whether these peaks are invariants of the blood distribution system as a whole, and whether and how the oscillatory components interact and synchronize.

Observations. To address these questions, we have analysed several noninvasively measured signals of cardiovascular origin recorded *simultaneously* at different sites of the human body. Because our primary interest centres on the dynamics of blood distribution, the time scale of observation was adjusted to estimate optimally all oscillations with a repetition time up to $\sim$1 minute – the average time taken for one circulatory cycle of blood through the system of a relaxed healthy subject.

The electrical activity of the heart (measured as an electrocardiogram, or ECG), blood pressure, respiration and peripheral blood flow were measured. The ECG was recorded with electrodes on both shoulders and one below the heart. Piezoeletric sensors were used to detect the blood pressure and respiratory movements of the thorax. The peripheral blood flow was measured by use of the laser-Doppler technique. The heart rate variability (HRV), consisting of times between consecutive heart beats, was derived from the ECG.

The time series, recorded for 20 minutes, were analysed using linear and nonlinear methods [9, 11]. The autocorrelation functions of the time series measured from blood flow, blood pressure, ECG and respiration contain several almost periodic components. The calculation of Lyapunov exponents from the blood flow signal in the phase space has revealed the deterministic nature of this signal. However, transients, noise and nonstationarities, which are inherent to biological signals, restrict the application of phase space methods. Methods in the frequency domain, on the other hand, are less sensitive to noise and nonstationarities. There are two major difficulties related to the frequency analysis of such signals:

(i) time-variation of their characteristic frequencies, which demands an analysis in the time-frequency domain; and

(ii) the relatively broad frequency band within which characteristic peaks are expected, raising problems with respect to time and frequency resolution.

For these reasons the wavelet transform [12], a time-frequency method providing for the necessary resolution at both high and low frequencies, was used.

Oscillations and their characteristic frequencies. The peaks in spectra appear at similar, and in some cases even at exactly the same frequencies. Between 0.0095 Hz and 1.6 Hz four peaks can be observed in the HRV in all subjects, ~0.2 Hz, ~0.1 Hz ~0.03 Hz and ~0.01 Hz. In addition to these frequencies the blood flow spectra also contain the cardiac frequency which, in healthy subjects at rest, is centered at ~1.0 Hz. While the corresponding amplitudes may differ considerably, almost the same frequencies characterize all signals and can thus be taken as characteristic of the blood distribution system. Like the cardiac frequency, that of respiration can also be determined directly by monitoring the respiratory function and is ~0.2 Hz.

Several studies were conducted to address the question of the physiological origin of the low frequency oscillations. Those with a ~10 s period in the blood pressure and HRV have been studied in connection with blood pressure regulatory mechanisms [13]. They are a manifestation of the myogenic activity of the smooth muscle cells of resistive vessels. These cells respond continuously to changes in intravascular pressure [14]. The peak between 0.02 Hz and 0.04 Hz appears to be attributable to neurogenic regulation of the vessels' radii, since it has been found to disappear after denervation [15] and is significantly reduced in skin flaps [16]. In addition, a peak near 0.01 Hz was found in all cardiovascular signals: it was recently shown [17, 18] to be related to endothelial modulated metabolic activity.

Interactions and synchronization. Oscillations whose characteristic frequencies are manifested at the macroscopic level can mutually synchronize for a short instant of time, as was shown first for the oscillations generated by the cardiac and respiratory systems. Recently proposed methods for the detection of synchronization between irregular and non-stationary oscillators (see [20] and the references therein) have made it possible to conduct extensive analyses of the cardiorespiratory couplings and the appearance of episodes of synchronization has been reported in several studies [19, 20, 21].

Schäfer *et al* (1998) found well expressed synchronization in a group of young athletes. Our own results [21] show short episodes of synchronization in healthy relaxed subjects which did not, however, exceed 2 minutes within the 20 minutes of a recording.

The appearance and the extent of synchronization changes with the state of the system. For example, in a critically ill subject in coma no phase synchronization can be observed at any time [22]: the cardiac and the respiratory systems seem to be disconnected from the rest of the cardiovascular system, as well as from their possible mutual influences, resulting in a virtually constant cardiac frequency and no relationship between their phases.

Recent studies have illuminated the way in which the pattern of phase synchronization changes during anaesthesia [23]. The two systems pass reversibly through a sequence of phase-synchronized states as the anaesthesia level changes, indicating that they can undergo phase transition like phenomena.

We have also studied the spatial synchronization of oscillations in the cardiovascular system [24]. Perhaps not surprisingly, the analysis has revealed that the cardiac oscillations, as observed at different sites of the system and in different physiological functions, are strongly synchronized. The same is true of the respiratory oscillations, regardless of where observed. Spatial synchronization of the slower oscillations that originate locally is weaker.

Coupled oscillators. The dynamics of the different physiological subsystems constituting the cardiovascular system are manifested on widely differing timescales. But in all cases – not just the heart and respiration – they are characterised by slowly varying frequencies and amplitudes, processes that are evidently a characteristic feature of the dynamics of the blood distribution system as a whole.

The results suggest that the cardiovascular system as a whole, including the microcirculation, can usefully be treated as a single entity. The heart frequency and its variations are transmitted to the periphery by motion of the blood, and are thus observable in peripheral blood flow and blood pressure. The lower-frequency (myogenic, neurogenic and endothelial-related) local regulatory mechanisms modulate the flow and in turn affect the variability of the heart rate. It is the continuous circulation of blood through the system of closed tubes that coordinates the local regulatory activity of each mechanism and evidently synchronizes it for much of the time (since, otherwise, its signature would not be resolved in the HRV signal). The existence of preferential phase and frequency-locking among spatially distributed components of a particular mechanism is manifested as the single almost periodic process that we observe at the macroscopic level. In terms of frequencies, it is almost irrelevant at which point we observe the system, or which function we choose to measure: each regulatory mechanism is reflected on every site, and can be detected in each cardiovascular function; its amplitude may, however, differ with respect to the function and the site of observation.

The existence of oscillations and episodes of their phase synchronization can be accounted for within the hypothesis that the blood distribution system is governed by a set of five coupled nonlinear oscillators [11, 22]. The amplitude/frequency wandering then arises because of couplings between them, and it appears to reflect a complex combination of the possible interactions.

Acknowledgement. This work was supported by the Slovenian Ministry of Education, Science and Sport.

References

[1] Angelone A and Coulter N A (1964). *J. Appl. Physiol.*, **19**, 479–482.

[2] Davis C T M and Neilson J M M (1967). *J. Appl. Physiol.*, **22**, 947–955.

[3] Hales S (1733). *Statical Essays II, Haemastaticks*, (London: Innings Manby)

[4] Penaz J, Roukenz J, and Waal H J (1968). In Drischel H and Tiedt N eds, *Byokibernetik*, (Karl Marx University, Leipzig), 233–236.

[5] Sayers M McA (1973). *Ergonomics*, **16**, 16–17.

[6] Akselrod S, Gordon D, Ubel F A, Shannon D C, Berger A C, and Choen R J (1981). *Science*, **213**, 220–222.

[7] Di Renzo M, Parati G, Pedotti A, and Zanchetti A, eds (1997). *Frontiers of Blood Pressure and Heart Rate Analysis*, (IOS Press, Amsterdam)

[8] Hoffman U, Yanar A, Franzeck U K, Edvards J M, and Bollinger A (1990). *Microvasc. Res.*, **40**, 293–301.

[9] Stefanovska A and Krošelj P (1997). *Open Systems and Information Dynamics*, **4**, 457–478.

[10] Bračič M and Stefanovska A (1998). *Bull. Math. Biol.* **60** 919–935.

[11] Stefanovska A and Bračič M (1999). *Contemporary Physics*, **40**, 31–55.

[12] Morlet J (1983). In Chen C H ed, *Issues in Acoustic Signal/Image Processing and Recognition*, NATO ASI Series, Vol.I, (Springer-Verlag, Berlin).

[13] Hyndman B W, Kitney R I, and Sayers B McA (1971). *Nature*, **233**, 339–341.

[14] Johnson P C (1991). *NIPS*, **6**, 41–42.

[15] Kastrup J, Bühlow J, and Lassen N A (1989). *Int. J. Microcirc.: Clin. Exp.*, **8**, 205–215.

[16] Söderström T, Stefanovska A, Veber M, and Svensson H (2001). *Am. J. Physiol., Heart and Circ. Physiol.*, accepted.

[17] Kvernmo H D, Stefanovska A, Kirkebøen K A, and Kvernebo K (1999). *Microvasc. Res.*, **57**, 298-309.

[18] Stefanovska A, Bračič M, and Kvernmo H D (1999). *IEEE Trans. Biomed. Eng.*, **46**, 1230-1239.

[19] Schäfer C, Rosenblum M G, Kurths J, and Abel H H (1998). *Nature*, **293**, 239–240.

[20] Rosenblum M G, Pikovsky A S, Schäfer C, Tass P, and Kurths J, (2000). In Moss F and Gielen S, eds, *Handbook of Biological Physics*, (Elsevier Science), 279–321.

[21] Bračič Lotrič M and Stefanovska A (2000). *Physica A*, **283**, 451–461.

[22] Stefanovska A, Bračič Lotrič M, Strle S, and Haken H (2001). *Physiol. Meas.*, **22**, 535–550.

[23] Stefanovska A, Haken H, McClintock P V E, Hožič M, Bajrovič F, and Ribarič S (2000). *Phys. Rev. Lett.*, **85**, 4831–4834.

[24] Stefanovska A and Hožič (2000). *Progr. Theor. Phys. Suppl.*, **139**, 270–282.

E-mail for Maja Bračič Lotrič : `maja@osc.fe.uni-lj.si`

Aneta Stefanovska,[1] **Dmitrii G Luchinsky,**[2] **and Peter V. E. McClintock** [2]

E-Mail: aneta@osc.fe.uni-lj.si

Nonlinear Dynamics and Synergetics
Faculty of Electrical Engineering, University of Ljubljana
Tržaška 25, 1000 Ljubljana, Slovenia[1]
Department of Physics, University of Lancaster, Lancaster LA1 4YB, UK [2]

The cardiovascular system as a system of coupled oscillators

Abstract. We present a modelling approach to the cardiovascular system, treating it as a system of coupled oscillators. It concentrates on the oscillatory nature of the dynamics on the time-scale of one average circulation period. The aim is to develop the simplest possible model that is able to reflect the oscillatory character of cardiovascular dynamics and is capable of reproducing the main statistical and dynamical features characteristic of the measured time series. These include the form of the spectra and the frequency/amplitude variations of the heart rate, respiration, blood flow and blood pressure, and the main features of the synchronization phenomena that are observed experimentally.

Introduction. The model synthesis was based upon the experimental observation that there are *five* main frequency components in various physiological time series: blood pressure, blood flow, ECG and respiration [1]. Accordingly, a system of five coupled oscillators was chosen to model the dynamics [2].

It is well-known that time delays are very important in the description of physiological systems and are often used in modelling individual components of the cardiovascular system [3]–[11]. In our approach, however, we perceive the blood distribution system as one in which continuous information about every subsystem, acting with essentially different frequencies, is provided and fed back via coupling terms, automatically yielding a hierarchy of delays corresponding to the time scale on which each particular subsystem acts.

Subsystems. The basic unit in the model, corresponding to the autonomous part of the oscillator, possesses the properties of structural stability, robustness and symmetry that are consistent with physiological understanding, and with the analyses of measured time series:

$$\begin{aligned}
\dot{x}_i &= -x_i q_i - \omega_i y_i + g_{x_i}(\mathbf{x}), \\
\dot{y}_i &= -y_i q_i + \omega_i x_i + g_{y_i}(\mathbf{y}), \\
q_i &= \alpha_i(\sqrt{x_i^2 + y_i^2} - a_i).
\end{aligned}$$

where $\mathbf{x}, \mathbf{y}$ are vectors of oscillator state variables, α_i, a_i, and ω_i are constants and $g_{yi}(\mathbf{y})$ and $g_{xi}(\mathbf{x})$ are linear coupling vectors. The activity of each subsystem is described by two state variables, the blood flow x_i, and the velocity of flow y_i, where i denotes the i-th oscillator corresponding to one of the physiological systems, viz. the cardiac, respiratory, myogenic, neurogenic or endothelial-mediated metabolic activities. The impact of other subsystems, acting on slower time scales, is taken into account as coupling terms and/or as random noise.

Couplings. A key feature of the model synthesis is the treatment of the couplings between oscillators. The nature of the couplings is currently unknown for most of the relationships between the subsystems. For simplicity, therefore, we use linear couplings – further justified by the observation of the same basic frequency components in all the physiological signals, and by the fact that only very small amplitude combinatorial components are observed.

In some cases, the sign of the coupling term can be determined from existing physiological knowledge and experimental observations. Direct modulation of the heart frequency by respiration, and clear evidence of the corresponding combinational frequencies in the Fourier spectra for the subject in coma, suggest that unidirectional parametric coupling, i.e. the cardiac frequency modified by respiration, but not vice versa, must be included in the model. Moreover, the experimental evidence also suggests that most of the other couplings are also asymmetrical. Additional difficulties in the model synthesis are related to the fact that the myogenic, neurogenic and metabolic activities cannot be measured directly in physiological experiments using noninvasive techniques.

Preliminary results of numerical simulations. We have carried out digital simulations of the model proposed in detail in [2]. To simplify manipulations with the multi-dimensional coupling we have built a MatLab based graphical user interface providing for real time control of all the parameters of the system.

The results, presented in [12], suggest that the type and strength of the linear coupling in our model can be determined quite accurately through comparison of the observed and simulated time series. We find that, in order to reproduce the main dynamical features of the cardiac rhythmic activity, both linear and parametric couplings must be taken into account, with the linear couplings being dominant. Fluctuations are found to play an important role in the dynamics of the cardiovascular system: they are responsible, at least in part, not only for the experimentally observed and numerically reproduced broadening of the main spectral peaks, but also for a number of regimes of synchronization. In particular, we note that the model is capable of reproducing the different synchrogramme patterns of observed experimentally including e.g. the standard phase-locked regime and the regime of continuously varying phase both in the presence and in the absence of noise. We were specially interested in establishing whether or not it is possible to reproduce the regime where there are short epochs of synchronization. It turns out that such behaviour can be reproduced numerically *only* in the presence of fluctuations.

Acknowledgements. The research was supported by the Royal Society of London, the Slovenian Ministry of Education, Science and Sport, the Engineering and Physical Sciences Research Council (UK), the Medical Research Council (UK) and INTAS.

References

[1] A Stefanovska and M Bračič (1999). *Contemp. Phys.* **40**, 31–55.

[2] A Stefanovska, M Bračič Lotrič, S Strle, and H Haken (2001). *Physiol. Meas.* **22**, 535–550.

[3] B W Hyndman, R I Kitney, and B McA Sayers (1971). *Nature* **233**, 339–341.

[4] R I Kitney, T Fulton, A H McDonald, and D A Linkens (1985). *J. Biomed. Eng.* **7**, 217–224.

[5] R W deBoer, J M Karemaker and J Strackee (1987). *Am. J. Physiol.* **253**, H680-H698.

[6] G. Baselli, S. Cerutti, S. Civardi, A. Malliani and M. Pagani (1988). *IEEE Trans. Biopmed. Eng.*, **35**, 1033–1046.

[7] J P Saul, R D Berger, P Albrecht, S P Stein, M Hui Chen and R J Choen (1991). *Am. J. Physiol.* **261**, H1231–H1245.

[8] J Starkee and N Westerhof eds (1993). *The physics of heart and circulation*, IoP, Bristol.

[9] B J TenVoorde, Th J C Faes, T W J Jansen, G J Scheffer and O Rompelman (1995). In *Computer Analysis of Cardiovascular Signals*, eds. M Di Renzo *et al*, IOS Press, Amsterdam, 119–134.

[10] H Seidel and H Herzel H (1995). In *Dynamical phenomena in living systems*, eds. E Mosekilde and O G Mouritsen, Springer, Berlin.

[11] A Cavalcanti and E Belardinelli (19996). *IEEE Trans. Biomed. Eng.* **43**, 982–989.

[12] A Stefanovska, D G Luchinsky and P V E McClintock (2001). *Physiol. Meas.* **22**, 551–564.

E-mail for: Dmitrii G Luchinsky and Peter V. E. McClintock
`d.luchinsky@lancaster.ac.uk, p.v.e.mcclintock@lancaster.ac.uk`

Hien Tran[1] and Jerry Batzel [2]
E-Mail: tran@contro.ncsu.edu

Dept. of Mathematics, North Carolina State University[1]
SFB Optimization and Control, Univ. Graz [2]

Modeling and analysis of instability in human respiration

Mathematical models of the human respiratory control system have been developed since 1940 to study a wide range of features of this complex system. In the absence of voluntary or neurological control, the respiratory control system in which we are concerned, varies the ventilation rate in response to the levels of CO_2 and O_2 in the body (chemical control). The model we are studying was proposed by Khoo et al. [9] and consists of a nonlinear system of delay differential equations with multiple delays building on the work of Grodins et al. [6]. Using this basic model we have:

- incorporated variable cardiac output using a model given in [5] thereby allowing the inclusion of variable delay in the feedback control loop;
- extended the model to study infant sleep respiratory patterns including apnea which may play a role in sudden infant death syndrome (SIDS);
- studied stability analytically using a reduced order model-based criteria for delay induced instability.

The respiratory control system mechanism acts by means of negative feedback. Deviations in blood gas partial pressures P_{CO_2}, P_{O_2}, from their physiological set points induce changes in ventilation rates which tend to compensate for these deviations. As chemosensors are a physical distance from the lungs, delays in this feedback can induce instabilities.

Periodic breathing (PB) is the generic name given to a number of breathing patterns which are involuntary and have a regular pattern. These patterns appear in patients with brain stem lesions, patients with congestive heart problems, normal individuals during sleep and at high altitudes, and newborn infants (which may be related to SIDS).

Perhaps the most widely held theory, introduced by Haldane and Douglas in 1909 holds that PB is caused by instability in the respiratory control system. It appears that PB is mediated by the peripheral sensory mechanism and is effected by delay in the feedback control loop and large deviations in the controller gain. Furthermore, apnea (lack of ventilation) can occur when the oscillations in the ventilatory control signal drive the signal to the cutoff point.

Delay is introduced into the control system due to the physical distance which CO_2 and O_2 levels must be transported to the sensory sites before the ventilatory response can be adjusted. The delay in transfer of partial pressure information for carbon dioxide (P_{CO_2}) and oxygen (P_{O_2}) from lung to chemosensors depends on cardiac output $\dot{Q}$ in general and blood flow rate to the brain $\dot{Q}_B$ in particular. Considered as a dynamical system with delay, well known mathematical results such as given in [3] show that long delay times in the feedback control loop will destabilize a system and produce oscillations. Figure (1) shows a schematic diagram of the three compartments of the model with the delays incorporated. These delays vary with blood flow. The compartments track arterial and venous partial pressures ($P_{a_{CO_2}}$, $P_{a_{O_2}}$, $P_{V_{CO_2}}$ $P_{V_{O_2}}$, and $P_{B_{CO_2}}$). In essence, this model represents a system of five nonlinear differential equations with four delays which are state dependent and distributed. Numerical and analytical results for such systems are difficult to obtain. See, e.g., [11]. The mathematical model is derived from straight-forward applications of mass balance equations and are given by:

$$\frac{d\mathrm{Pa}_{\mathrm{CO_2}}(t)}{dt} = \frac{863\dot{\mathrm{Q}}\mathrm{K}_{\mathrm{CO_2}}[\mathrm{P}_{\mathrm{V}_{\mathrm{CO_2}}}(t-\tau_{\mathrm{V}}) - \mathrm{Pa}_{\mathrm{CO_2}}(t)]}{\mathrm{M}_{\mathrm{L}_{\mathrm{CO_2}}}} + \frac{\mathrm{E_F}\dot{\mathrm{V}}_{\mathrm{I}}[\mathrm{P}_{\mathrm{I}_{\mathrm{CO_2}}} - \mathrm{Pa}_{\mathrm{CO_2}}(t)]}{\mathrm{M}_{\mathrm{L}_{\mathrm{CO_2}}}}, \tag{1}$$

$$\frac{d\mathrm{Pa}_{\mathrm{O_2}}(t)}{dt} = \frac{863\dot{\mathrm{Q}}[\mathrm{m_v}\mathrm{P}_{\mathrm{V}_{\mathrm{O_2}}}(t-\tau_{\mathrm{V}}) - \mathrm{m_a}\mathrm{Pa}_{\mathrm{O_2}}(t) + \mathrm{B_v} - \mathrm{B_a}]}{\mathrm{M}_{\mathrm{L}_{\mathrm{O_2}}}} + \frac{\mathrm{E_F}\dot{\mathrm{V}}_{\mathrm{I}}[\mathrm{P}_{\mathrm{I}_{\mathrm{O_2}}} - \mathrm{Pa}_{\mathrm{O_2}}(t)]}{\mathrm{M}_{\mathrm{L}_{\mathrm{O_2}}}}, \tag{2}$$

$$\frac{d\mathrm{P}_{\mathrm{B}_{\mathrm{CO_2}}}(t)}{dt} = \frac{\mathrm{MR}_{\mathrm{B}_{\mathrm{CO_2}}}}{\mathrm{M}_{\mathrm{B}_{\mathrm{CO_2}}}\mathrm{K}_{\mathrm{B}_{\mathrm{CO_2}}}} + \frac{[\dot{\mathrm{Q}}_{\mathrm{B}}(\mathrm{Pa}_{\mathrm{CO_2}}(t-\tau_{\mathrm{B}}) - \mathrm{P}_{\mathrm{B}_{\mathrm{CO_2}}}(t))]}{\mathrm{M}_{\mathrm{B}_{\mathrm{CO_2}}}}, \tag{3}$$

$$\frac{d\mathrm{P}_{\mathrm{V}_{\mathrm{CO_2}}}(t)}{dt} = \frac{\mathrm{MR}_{\mathrm{T}_{\mathrm{CO_2}}}}{\mathrm{M}_{\mathrm{T}_{\mathrm{CO_2}}}\mathrm{K}_{\mathrm{CO_2}}} + \frac{[\dot{\mathrm{Q}}_{\mathrm{T}}(\mathrm{Pa}_{\mathrm{CO_2}}(t-\tau_{\mathrm{T}}) - \mathrm{P}_{\mathrm{V}_{\mathrm{CO_2}}}(t))]}{\mathrm{M}_{\mathrm{T}_{\mathrm{CO_2}}}}, \tag{4}$$

$$\frac{d\mathrm{P}_{\mathrm{V}_{\mathrm{O_2}}}(t)}{dt} = \frac{\dot{\mathrm{Q}}_{\mathrm{T}}[\mathrm{m_a}\mathrm{Pa}_{\mathrm{O_2}}(t-\tau_{\mathrm{T}}) - \mathrm{m_v}\mathrm{P}_{\mathrm{V}_{\mathrm{O_2}}}(t) + \mathrm{B_a} - \mathrm{B_v}] - \mathrm{MR}_{\mathrm{T}_{\mathrm{O_2}}}}{\mathrm{M}_{\mathrm{T}_{\mathrm{O_2}}}\mathrm{m_v}}. \tag{5}$$

The control function $\dot{\mathrm{V}}_{\mathrm{I}}$ in the above equations is derived based on the following observations (among others):

- The central controller responds exclusively to $\mathrm{P}_{\mathrm{CO_2}}$ [12].
- The peripheral controller responds to $\mathrm{P}_{\mathrm{CO_2}}$ and $\mathrm{P}_{\mathrm{O_2}}$ [12].
- The effect of $\mathrm{P}_{\mathrm{O_2}}$ on $\dot{\mathrm{V}}_{\mathrm{I}}$ for fixed $\mathrm{P}_{\mathrm{CO_2}}$ is exponential [12].
- Berger and West [2, 12] indicate that the peripheral $\mathrm{P}_{\mathrm{O_2}}$ interacts multiplicatively with the peripheral $\mathrm{P}_{\mathrm{CO_2}}$ effect.
- The peripheral and central control effects are additive [4].

Taking these facts into consideration, the control takes the form:

$$\dot{\mathrm{V}}_{\mathrm{I}} = \mathrm{G_P}\exp(-.05\mathrm{Pa}_{\mathrm{O_2}}(t-\tau_{\mathrm{a}}))(\mathrm{Pa}_{\mathrm{CO_2}}(t-\tau_{\mathrm{a}}) - \mathrm{I_P}) + \mathrm{G_C}(\mathrm{P}_{\mathrm{B}_{\mathrm{CO_2}}}(t) - \frac{\mathrm{MR}_{\mathrm{B}_{\mathrm{CO_2}}}}{\mathrm{K}_{\mathrm{CO_2}}\dot{\mathrm{Q}}_{\mathrm{B}}} - \mathrm{I_C}),$$

where $\dot{\mathrm{V}}_{\mathrm{I}}$ is minute ventilation, $\mathrm{I_C}$ and $\mathrm{I_P}$ are apneic thresholds, $\mathrm{G_C}$ and $\mathrm{G_P}$ are controller gains. We refer the interested reader to the recent article [1] for more details on these and other aspects of the model.

The sleep condition involves a number of different states and stages with different physiological profiles. As one passes from stage 1 (S1) to stage 4 (S4) non rapid eye movement (NON-REM) sleep the $\mathrm{CO_2}$ response curve shifts rightward, response to overall ventilatory drive diminishes, and muscle resistance to the upper airways and other muscle groups related to breathing increases. These effects are referred to as loss of the "wakefulness stimulus" [8]. Metabolic rates and cardiac output are also diminished. Once stage 4 is reached the sleeper shifts between NON-REM and rapid eye movement (REM) sleep. These physiological changes affect the stability of the respiratory control system. In 1991, Khoo [8] extended the basic model to simulate respiration during sleep reflecting these transitional features. We adapted this model for our infant sleep respiration study.

The occurrence of PB and apnea during sleep is related to the number of changes in the control response which occur during sleep as described above.

In this model we consider only the withdrawal of the wakefulness stimulus sufficient to produce transient reduction in ventilatory drive past a minimal threshold. This will be interpreted as a central apnea. We will assume that this apneic episode will terminate only with arousal. Arousal will be triggered by the chemical ventilatory stimulus rising above an arousal threshold level. Arousal will reset the control mechanism to its awake parameter values.

In modeling the respiratory processes of full term infants in the age range of 3-4 months we use allometric scaling for physical parameters. Allowance is made for an alveolar-capillary gradient $D_{\text{A-cap}}$ for P_{O_2} [10], shunted blood flow from the systemic venous return to systemic arterial blood flow, and changes in hemoglobin loading characteristics (via dissociation laws).

These modeling studies looked at the effects on respiratory stability of arousal thresholds, rightward shifts in ventilatory drive due to the withdrawal of the awake stimulus, increase in the minimal threshold for ventilation, and loss of ventilatory drive during sleep.

Figure (2) reflects blood gas variation when apnea occurs due to ventilatory drive dropping to a level sufficiently low such that respiratory muscle response is absent and a central apneic episode begins. A fast transition time to the sleep state and increased maximal shift S_w (approximately equal to the awake ventilatory drive [8]) and an increase in arousal threshold produces this case. The resulting apnea causes ventilatory drive to rise until arousal occurs. The disturbance to blood gas levels is sufficient to produce new cycles of apnea.

Three-Dimensional State Space Model Stability Analysis

To consider analytically the stability of this model we considered a three-dimensional reduced order model based on the following assumptions:

(i) $P_{V_{CO_2}}$ = constant.

(ii) $P_{V_{O_2}}$ = constant.

(iii) $\dot{Q}$ = constant.

(iv) Only one constant delay is considered: $\dot{Q}$ is held constant, while the peripheral and central delay are assumed equal.

The reduced order model has three equations represent lung and brain P_{CO_2} and P_{O_2} as in equations (1)-(3) while the tissue equations are replaced by assumptions (i) and (ii) above. With $x(t)$ and $y(t)$ representing respectively $P_{a_{CO_2}}$ and $P_{a_{O_2}}$ deviations from ambient level, $z(t)$ representing $P_{B_{CO_2}}$, and V ventilation, the equations take the form:

$$\frac{d\mathrm{x}(t)}{dt} = \mathrm{a}_1 - \mathrm{a}_2\mathrm{x}(t) - \mathrm{a}_3\mathrm{V}\mathrm{x}(t), \tag{6}$$

$$\frac{d\mathrm{y}(t)}{dt} = \mathrm{b}_1 - \mathrm{b}_2\mathrm{y}(t) - \mathrm{b}_3\mathrm{V}\mathrm{y}(t), \tag{7}$$

$$\frac{d\mathrm{z}(t)}{dt} = \mathrm{c}_1 + \mathrm{c}_2\mathrm{x}(t-\tau) - \mathrm{c}_2\mathrm{z}(t), \tag{8}$$

where the a_i, b_i, and c_i, are accumulated constants. V takes the form discussed above:

$$\mathrm{V} = \mathrm{G_c}(\mathrm{z}(t) - \frac{\mathrm{c}_1}{\mathrm{c}_2} - \mathrm{I_c}) + \mathrm{G_p}\exp -0.05(\mathrm{P}_{\mathrm{I}_{\mathrm{O}_2}} - \mathrm{y}(t-\tau))(\mathrm{x}(t-\tau) - \mathrm{I_p}).$$

Using standard arguments one can obtain the following results:

Theorem. *The system (6), (7) and (8) has a unique solution for initial point $\sigma \in \mathbb{R}$ and initial function $\phi \in C$.*

Furthermore, from Theorem 2.2.2 in [7], we are also guaranteed that the solutions are continuously dependent on initial data so that the model is well-posed.

Theorem. *The above system described by (6),(7) and (8) has a unique positive equilibrium $(\bar{x}^*, \bar{y}^*, \bar{z}^*)$.*

We next linearize equations (6), (7) and (8) about the equilibrium solution and derive the following characteristic equation:

$$\Delta(\lambda, \tau) = \mathrm{P}(\lambda) + \mathrm{Q}(\lambda)e^{-\tau\lambda} = 0. \tag{9}$$

Applying Theorem 3.5 described in Cooke and van den Driessche [3] we look for τ which will produce instability. There will be one cross over from stable to unstable behavior. The overall structure of instability is illuminated by the three-dimensional model while the actual state variables were in good agreement with the five-dimensional model.

Based on the foregoing development, we can show that:

1. The central control acts to reduce the instability inherent in the peripheral control mechanism. The peripheral control responds quickly to changes in the blood gases while the central control responds more slowly and with less variation due to the process of transforming $\mathrm{Pa}_{\mathrm{CO}_2}$ levels into $\mathrm{P}_{\mathrm{B}_{\mathrm{CO}_2}}$ levels.

2. The lung compartments act to dampen oscillations and contribute to stability, as Table 1 indicates.

3. Variations in controller gain are critical to the stability of the system.

4. A control which varies depth of breathing is more unstable than one which varies rate of breathing.

Tables (1) and (2) provide numerical results for this analysis. In these tables the **critical values** are defined as multiples of **normal values** which produce instability. For example,"control multipliers" refer to multiples of normal gains and "τ multipliers" represent multipliers of the nominal case delay time τ. Thus a τ multiplier of 5.5 implies that we must increase the normal case delay τ five and a half times for instability in the studied case. Table 1 compares the impact of controlling minute ventilation by changes rate and depth of breathing. Dead space ventilation can be modeled as a % reduction via a multiplier E_F of V or as a subtraction of a fixed volume V_D from V. The former would model ventilation which is changed by varying the rate of breathing (a fixed % of minute ventilation is wasted) while the later would represent a fixed breathing rate with changes in ventilation the result of varying the depth of a breath (fixed dead space volume lost per breath). Table 2 compares the impact of reduced cardiac output (increased delay) as found in congestive heart failure. Note that, as Figure (3) indicates, the increased delay produces oscillations. For control gain $2.5\times$ normal, the destabilizing delay is less than the normal delay. Here, Chenyne-Stokes type respiration occurs.

References

[1] J. J. Batzel, H. T. Tran, *Modeling instability in the control system for human respiration: applications to infant non-rem sleep*, Applied Mathematics and Computation, Vol. 110, 2000, pp. 1-51.

[2] A. Berger, R. Mitchell, and J. Severinghaus, *Regulation of respiration*, New England J. Medicine, Vol. 297(4), 1977, pp. 194-201.

[3] K. Cooke and P. van den Driessche, *On zeroes of some transcendental equations*, Funckialaj Ekvacioj 29, pp. 77-90,1986.

[4] D. C. Cunningham, P. A. Robbins, and C. B. Wolff, *Integration of respiratory responses* in A. P. Fishman editor *Handbook of Physiology: the respiratory system, Part II*, pp. 475-528, American Physiological Soc., Bethesda Md., 1986.

[5] W. F. Fincham and F. T. Tehrani, *On the regulation of cardiac output and cerebral blood flow*, J. Biomed. Eng, Vol. 5, 1983, pp. 73-75.

[6] F. S. Grodins, J. S. Gray, K. R. Schroeder, A. I. Norris, R. W. Jones, *Respiratory responses to CO_2 inhalation: a theoretical study of a nonlinear biological regulator*, J. Appl Physiology, 7, pp. 283-308, 1954.

[7] J. K. Hale and S. M. Verduyn Lunel, *Introduction to Functional Differential Equations*, Springer-Verlag, N.Y. 1993.

[8] M. C. K. Khoo, A. Gottschalk, and A. I. Pack, *Sleep-induced periodic breathing and apnea: a theoretical study*, J. Appl. Physiol. 70(5), pp. 2014-2024, 1991.

[9] M. C. K. Khoo, R. E. Kronauer, K. P. Strohl, and A. S. Slutsky, *Factors inducing periodic breathing in humans: a general model*, J. Appl. Physiology, 53(3), pp. 644-659, 1982.

[10] G. Koch, *Alveolar ventilation, diffusing capacity and the A-a PaO_2 difference in the newborn infant*, Respir. Physiol. 4, pp. 168-192, 1968.

[11] J. Mallet-Paret, R. D. Nussbaum, P. Paraskevopoulos, *Periodic Solutions for functional differential equations with multiple state-dependent time lags*, Top.Methods Nonlinear Analy., 3(1), pp. 101-162, 1994.

[12] J. B. West, *Respiratory Physiology*, Williams and Co., 1977.

Table 1: Stability results of parameter changes for 3-D model

3-D with $E_F = 0.7$ (modulate rate of breathing)		
Quantity	parameter multiplier	τ multiplier
G_P and G_C	1.0	11.26 x
G_P and G_C	2.0	5.5 x
$M_{L_{CO_2}}$ and $M_{L_{O_2}}$	0.5	10.99 x
$M_{L_{CO_2}}$ and $M_{L_{O_2}}$	2.0	12.6 x
3-D with $V_D = 2.0$ l/min (modulate depth of breathing)		
Quantity	parameter multiplier	τ multiplier
G_P and G_C	1.0	5.67 x
G_P and G_C	2.0	3.09 x
$M_{L_{CO_2}}$ and $M_{L_{O_2}}$	0.5	4.5 x
$M_{L_{CO_2}}$ and $M_{L_{O_2}}$	2.0	7.05 x

Table 2: Stability calculation model parameter base values for Fig. 3

Figure 3	Quantity	Unit	Value
	G_P	l/min/mm Hg	112.5
	G_C	l/min/mm Hg	3.0
	$\dot{Q}$	l/min	3.5
	normal τ	sec	14.6
	unstable τ multiple at normal gain	...	1.76
	unstable τ multiple at 2.5 x normal gain	....	0.77
	$\dot{V}_D$	l/min	2.00

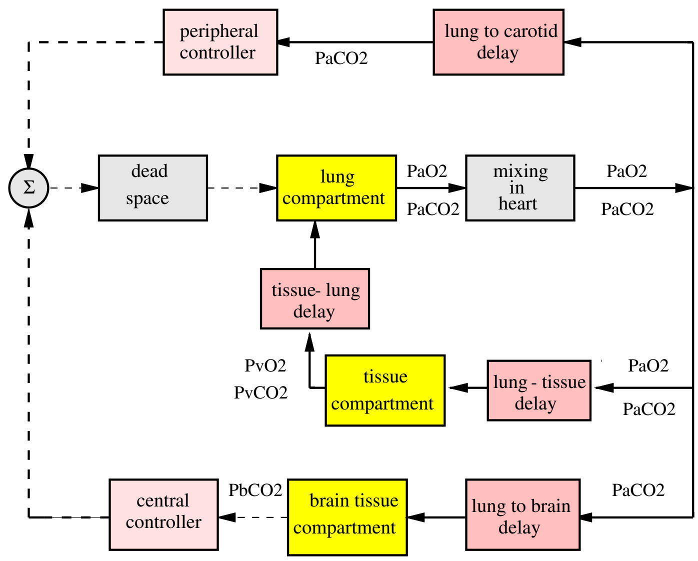

Figure 1: Block diagram of the respiratory system model

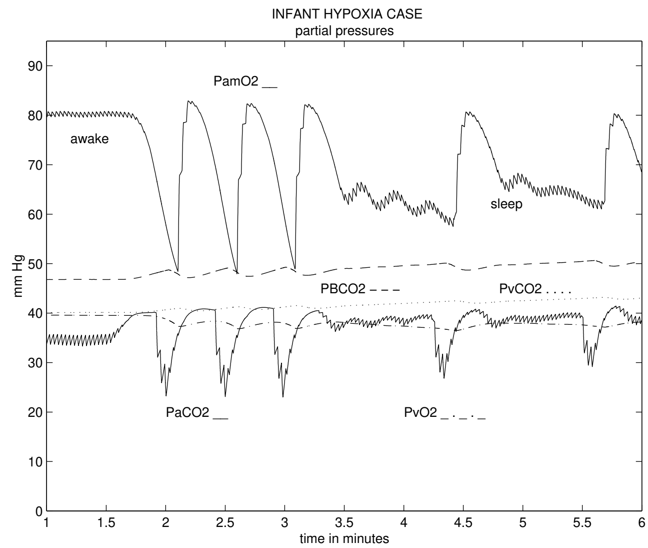

Figure 2: Infant blood gas level destabilized by sleep transition

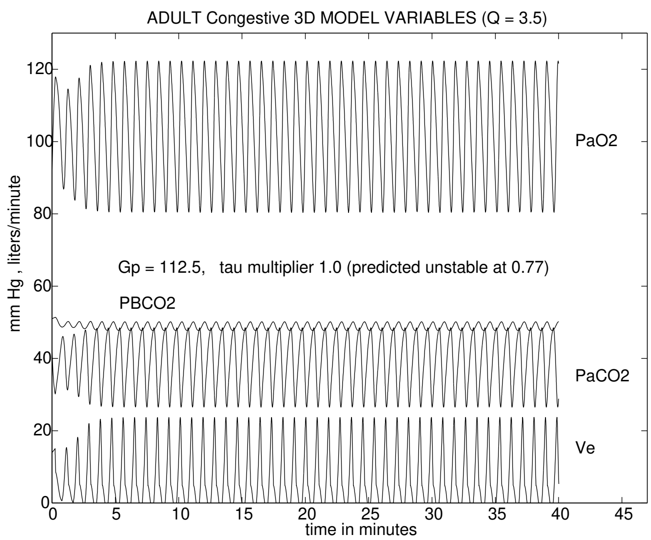

Figure 3: Congestive heart condition: cardiac output 3.5 l/min and high gain

Mauro Ursino and Elisa Magosso
E-Mail: mursino@deis.unibo.it

Dept. of Electronics, Computer Science and Systems
University of Bologna

A mathematical analysis of short-term cardiovascular regulation during changes in blood gas content and exercise

Acute changes in arterial oxygen and carbon dioxide pressures have a strong impact on cardiovascular parameters. Various local and reflex mechanisms, in fact, are triggered in response to alterations in blood gas content, in an effort to maintain oxygen delivery and CO_2 withdrawal adequate to the metabolic need. These mechanisms include local vasodilation in peripheral vessels, the arterial chemoreflex, ventilatory adjustments with consequent activation of the lung-stretch receptor reflex, and a direct response of the CNS to gas tensions in the medulla [1]. Moreover, alterations in systemic arterial pressure, which usually ensue from the previous adjustments, activate the baroreflex control system as well. Similarly, physical activity mostly challenges the regulatory abilities of the cardiorespiratory system. During exercise, the cardiovascular and respiratory systems must act in concert in order to supply adequate oxygen and nutrients to working muscles, sustain removal of carbon dioxide and other metabolic products, dissipate heat and, at the same time, maintain the requirements of other essential organs. To achieve this, dynamic exercise is accompanied by hyperpnea, increase in cardiac output, and redistribution of blood flow towards active muscles, mainly due to a strong decrease in their vascular resistance. As a consequence of skeletal muscle vasodilation, total peripheral resistance falls and mean arterial pressure only rises modestly. These cardiovascular adjustments result from a superimposition between extravascular mechanical effects of muscle contraction (the so called muscle pump), local vascular control processes and a reconfiguration of autonomic nervous activity [2]: in particular, sympathetic activity to heart and vessels increases, while cardiac vagal tone withdraws. Even though the mechanisms participating to cardiovascular control during changes in blood gas content and exercise have been known for many decades, a comprehensive mathematical analysis of the problem is still lacking. In this work we present the main aspects of an original mathematical model of the acute cardiovascular regulation. The purpose of this model is to summarize most of the present physiological knowledge in the field into a consistent theoretical framework. The controlled system (plant) includes the pulsating heart and the pulmonary and systemic circulation. This system has been extensively described in previous works, where more details can be found [3-5]. The regulatory actions working in response to changes in blood gas content are summarized in the block diagram of Fig. 1. They include the afferent information from several groups of receptors (arterial baroreceptors, peripheral chemoreceptors, lung-stretch receptors), the response of the central neural system to changes in O_2 and CO_2 tension, the activity of the efferent sympathetic fibers directed to the heart and peripheral vessels, the vagus activity, the response of various effectors to the efferent activity of neural fibers, the local effect of oxygen and CO_2 on peripheral resistances in the organs under local metabolic control and the ventilation response to peripheral and central chemoreceptor drive. Each mechanism in Fig. 1 is described mathematically according to data reported in the physiological literature [see 4-7]. The model is able to reproduce experimental data concerning the cardiovascular response to various combinations of blood gas derangement (normocapnic hypoxia, hypocapnic hypoxia, normoxic hypercapnia, hypoxic hypercapnia) [5-7]. An example is shown in Fig.2, where the simulated percentage changes of the main cardiovascular quantities (systemic arterial pressure, heart rate, cardiac output and systemic vascular resistance) in response to a hypocapnic hypoxia are shown and compared with experimental data in the dog [8]. During dynamical exercise, the regulatory actions working on cardiovascular parameters in the model involve also some additional mechanisms, i.e., the muscle pump, metabolic peripheral vasodilation, and the effect of a central command on the sympathetic and vagal activities [2, 9]. In particular, the mechanical effects of muscle contractions (muscle pump) have been simulated assuming that extravascular pressure outside active muscle veins (i. e., intramuscular pressure) changes periodically during exercise, and making use of a non-linear pressure-volume characteristic for the collapsing veins. According to experimental results, central command has an inhibitory effect on the vagus, while excites sympathetic activities [2]. The relationships between the central command and the efferent activities are monotonic functions of the relative exercise intensity, with a lower threshold and an upper saturation level. In order to reproduce muscle exercise hyperemia, we assumed that peripheral resistance in the active muscle compartment depends not only on neural influences, but also on local metabolic control mechanisms. The latter comprise the effect of increased oxygen consumption rate and of metabolic production of vasodilator substances, each described as a function of exercise intensity through a static characteristic and a first-order low-pass dynamic. The only input for the model is the relative intensity of aerobic exercise (I); a step change in this quantity triggers the central command and affects oxygen consumption rate and metabolite accumulation in the active skeletal muscle. At rest I is equal to 0, while at the anaerobic threshold I is conventionally set equal to 1. An example of model simulation of dynamical exercise is shown in Fig. 3, and compared with clinical data in humans [10]. This figure shows the percentage changes in heart rate, cardiac output, mean arterial pressure, systemic vascular conductance, and blood flow in active muscles plotted versus relative exercise intensity (I). The agreement between model predictions and clinical data is satisfactory. In conclusion, the present model is able to integrate the main mechanisms involved in the acute response to blood gas derangement and to dynamical exercise into a single theoretical setting. The simulation results show that the model is able to reproduce cardiovascular response in a large variety of experimental and/or clinical conditions. Moreover, the model underlines the extreme complexity of cardiovascular regulation, resulting from the non-linear interaction of many mechanisms (sometimes synergistic, sometimes antagonistic), simultaneously operating. At present, the model may be useful in the interpretation of experimental and clinical data, to improve our understanding of exercise physiology, and as an educational tool to analyze the complexity of cardiovascular and respiratory regulation.

References

1. Daly MB. *Peripheral arterial chemoreceptors and respiratory cardiovascular integration.* Oxford: Oxford University Press, 1997.

2. L.B. Rowell, *Human Cardiovascular Control*, New York: Oxford University Press, 1993.

3. Ursino M., Antonucci M., and Belardinelli E.. *The role of active changes in venous capacity by the carotid baroreflex: analysis with a mathematical model*, Am. J. Physiol. 267 (Heart Circ. Physiol. 36): H2531-H2546, 1994.

4. Ursino M. *Interaction between carotid baroregulation and the pulsating heart: a mathematical model.* Am. J. Physiol. 275 (Heart Circ. Physiol. 44): H1733-H1747, 1998.

5. Ursino M and Magosso E. *Acute cardiovascular response to isocapnic hypoxia. I: a mathematical model.* Am. J. Physiol. Heart Circ. Physiol.. 279: H149-H165, 2000a.

6. Ursino M and Magosso E. *Acute cardiovascular response to isocapnic hypoxia. II: model validation.* Am. J. Physiol. Heart Circ. Physiol. 279: H166-H175, 2000b.

7. Magosso E. and Ursino M. *A mathematical model of CO_2 effect on cardiovascular regulation.* Am. J. Physiol. Heart Circ. Physiol. 2001 (in press).

8. Kontos H.A., Levasseur J.E., Richardson D.W., Mauck H.P., and Patterson J.L., *Comparative circulatory responses to systemic hypoxia in man in ananesthetized dog.* J. Appl. Physiol., vol. 23 (3):381-386, 1967.

9. Magosso E., Felicani A., Ursino M. *A mathematical model of cardiovascular response to dynamic exercise.* Proceedings of the 23rd Annual International Conference of the IEEE Engineering in Medicine and Biology Society, Instanbul, October 2001.

10. J.A. Pawelczyk, B. Hanel, R.A. Pawelczyk, J. Warberg, and N.H. Secher, *Leg vasoconstriction during dynamic exercise with reduced cardiac output*, J. Appl. Physiol. 73(5): 1838-1846, 1992.

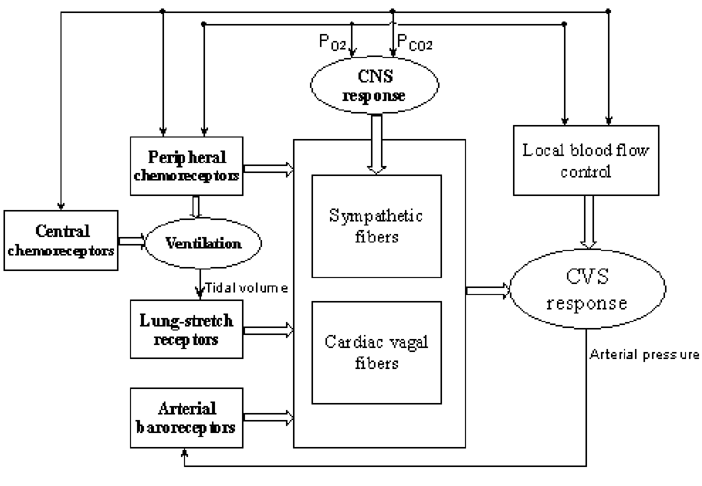

Figure 1:

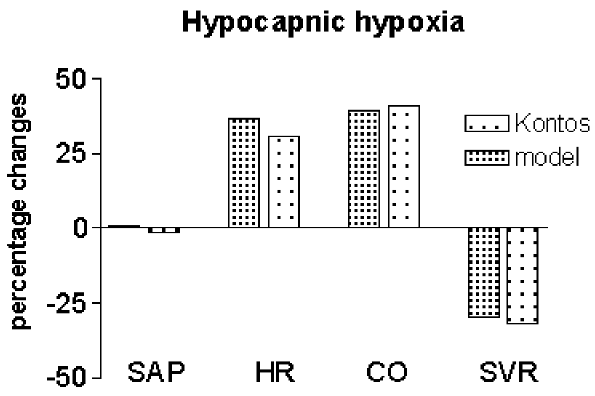

Figure 2:

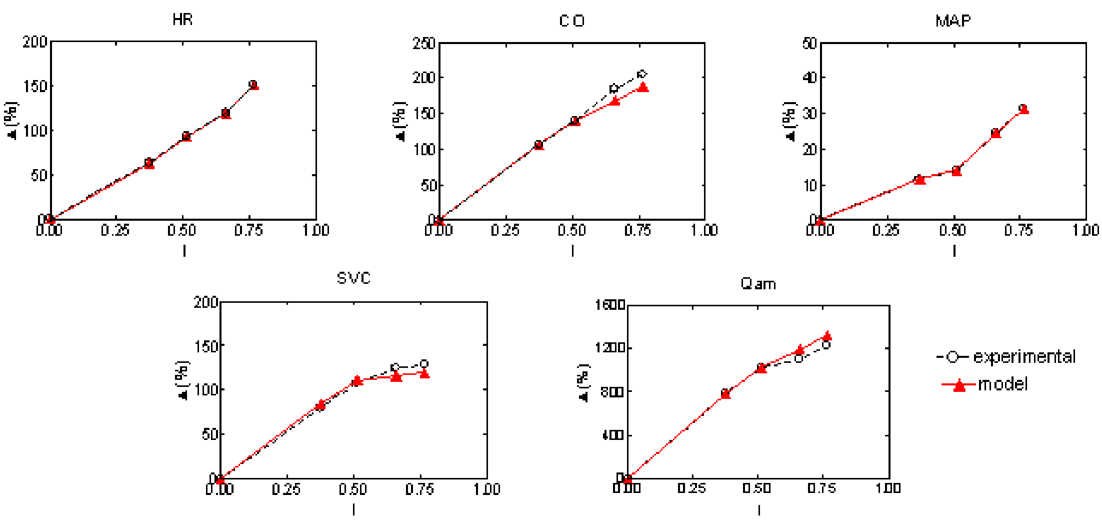

Figure 3:

Nico Westerhof,[1] Patrick Segers,[2] and Nikos Stergiopulos [3]
E-Mail: n.westerhof.physiol@med.vu.nl

Laboratory for Physiology
Institute for Cardiovascular Research
Free University Amsterdam[1]
Hydraulics Laboratory, Institute of Biomedical Technology
University of Gent, Belgium[2]
Biomedical Engineering Laboratory,
EPFL, Lausanne Switzerland [3]

Cardiac and arterial contribution to blood pressure in hypertension

Blood pressure results from the interaction of the heart, the pump, and the arterial system, the load. When the arterial load is increased, by either a larger peripheral resistance and/or decreased arterial compliance, and hypertension follows. Subsequently the heart will remodel or hypertrophy and later heart failure may result, leading to a life threatening condition. It is generally accepted that increases in load result in hypertrophy but the possible contribution of the hypertrophying heart is not considered. We therefore wondered if and how much the remodeled or hypertrophied heart contributes to blood pressure.

We constructed a simplified model of the heart and arterial load. The cardiac part of the model is based on the varying elastance concept (Suga et al., 1973) and is described with 3 parameters: diastolic (E_{min}) and end-systolic (E_{max}) pressure-volume relations, and the intercept of these relations with the volume axis (V_d). Venous return is represented by venous filling pressure (P_v). The normalized time-varying elastance curve ($E_N(t)$) is taken constant, i.e., independent of the cardiac remodeling process, on the basis of the report by Senzaki et al. (1996), where it was found that, in the human, the normalized curve is similar for normal and pathological conditions. The arterial load is modeled with a four-element windkessel model (Stergiopulos et al., 1999). This model, with a total of 8 parameters, was tested on human and animal data and shown to produce accurate aortic pressures and flows.

We used the data of Ganau et al. (1992) to derive the eight parameters for normotensive subjects and 4 groups of hypertensive subjects. The four groups of hypertensive patients reported in that paper were: normal left ventricle, concentric remodeling, concentric hypertrophy, and eccentric hypertrophy. Using the derived parameters the model accurately predicts the systolic and diastolic blood pressure for all these conditions. Using the model, and with the known parameters, we can now derive the individual contribution of the arterial load and of the heart to the systolic, diastolic and mean blood pressure. In the normotensive subjects blood pressure is 124/77 mmHg. In the following we report on changes in systolic pressure only. In the hypertensive patients with still normal left ventricle the systolic pressure is 145 mmHg. The increase of 21 mmHg is for about 50% due to the arterial load increase and about 50% due to the changed properties of the left ventricle. In concentric remodeling almost the entire pressure increase in systolic pressure results from the increased load alone. In concentric hypertrophy both the arterial load change and cardiac change contribute about equally to the systolic blood pressure increase. In eccentric hypertrophy the pressure increase is mainly the result of the change in cardiac pump function.

Another approach to study blood pressure is to describe the heart as a pump by means of the pressure-flow relation, the pump function curve (Elzinga and Westerhof, 1973) and describe the arterial system on basis of traveling waves. In hypertension, when wave speed and reflection are increased, the heart hypertrophies, which results in a pump function graph that approaches a flow source. With a flow source reflections have a stronger effect on aortic pressure, resulting in a higher systolic pressure (Westerhof and O'Rourke, 1995).

We conclude from both model approaches that when the heart remodels or hypertrophies the increased systolic blood pressure is not resulting from the increased arterial load alone but also results from the changed pump characteristics. Obviously these models are great simplifications of reality and are therefore limited. However, even the limited number of parameters required, have, to the best of our knowledge, never been determined in together in the human. It would be of enormous value if this would be done in the (cardiovascularly) healthy subject and in patients. Thus at present it is not possible or useful to make the models more sophisticated. First we need the basic parameters to study if improvement of the models is necessary. If indeed required the models then could be extended and then and make the predictions stronger.

References

1. Elzinga G, Westerhof N. *How to quantify pump function of the heart.* Circ Res 1979; 44:303-308.

2. Ganau A, Devereux RB, Roman MJ, de Simone G, Pickering TG, Saba PS, Vargiu P, Simongini I, Laragh JH. *Patterns of left ventricular hypertrophy and geometric remodeling in essential hypertension.* J Am Coll Cardiol 1992; 19: 1550 - 1558.

3. Senzaki H, Chen C-H, Kass DA. *Single-beat estimation of end-systolic pressure-volume relation in humans: a new method with the potential for noninvasive application.* Circulation 1996;94:2497- 2506.

4. Stergiopulos N, Westerhof BE, Westerhof N. *Total arterial inertance as the fourth element of the windkessel model.* Am J Physiol 1999; 276: H 81 - H88.

5. Suga H, Sagawa K, Shoukas AA. *Load independence of the instantaneous pressure-volume ratio of the canine left ventricle and effects of epinephrine and heart rate on the ratio.* Circ Res 1973; 32: 314 - 322.

6. Westerhof N. O'Rourke MF. *Hemodynamic basis for the development of left ventricular failure in systolic hypertension, and for its logical therapy.* J Hypertension 1995; 13: 943-952.

Joint work with: Patrick Segers ‡ Nikos Stergiopulos †

‡ *Hydraulics Laboratory, Institute of Biomedical Technology, University of Gent, Belgium*

† *Biomedical Engineering Laboratory, EPFL, Lausanne Switzerland*

Titles of workshop talks

1. G. Chauvet
   On the integration of physiological systems: the example of respiratory regulation

2. A. Fowler
   Mathematical modelling of respiratory control and the prediction of periodic breathing

3. M. Guevara
   Scale invariance in the cardiovascular system

4. D. Hoyer
   Evaluation of different types of cardiovascular-respiratory interdependencies - approaches by mutual information and phase synchronisation statistics.

5. E. Jung
   Simulations of valveless pumping using the Immersed Boundary Method: Parameter studies.

6. A. Leuprecht
   Computer simulations of blood flow in large arteries

7. A. Noordergraaf and J. Ottesen
   Implications of the integer ratio between cardiac and respiratory rates

8. A.V. Panfilov
   Electrophysiological model of the heart and its application to studying of cardiac arrhythmias

9. M. Rosenblum
   Quantitative analysis of cardiorespiratory interaction in healthy infants

10. L. Rowell
    Some crucial problems in cardiovascular control during exercise

11. W. Schreiner
    Modes of optimization of arterial tree models

12. A. Stefanovska
    The cardiovascular system as a system of coupled oscillators

13. H.T. Tran
    The human respiratory control system: models, applications, and analyses

14. J. Turi
    Feedback stabilization in differential equations with state-dependent delays

15. M. Ursino
    A Mathematical analysis of short-term cardiovascular regulation during changes in blood gas content and exercise

16. P. Wabel
    Model based control of hemodialysis

17. N. Westerhof
    Cardiac and arterial contribution to blood pressure in hypertension

18. R. Zietse
    Differences between our simulation study of intercompartmental fluid shifts during dialysis and the in vivo situation improve our understanding of dialysis

19. U. Zwiener
    Nonlinear dynamics in cardiovascular pathophysiology

Thanks

Special thanks to the following people who helped with this workshop: Stefan Volkwein, Georg Propst, Gerlinde Krois, Inge Puntigam, and Alex Kuntsevich for his poster design advice and help.

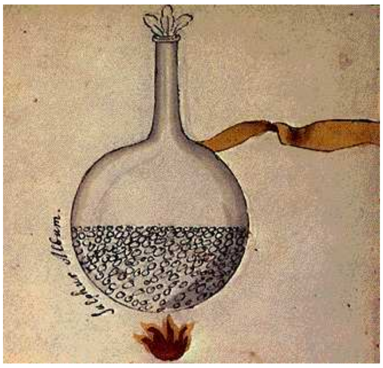

Special Research Center "Optimization and Control"

The special research center (SRC F-003) "Optimization and Control" focuses on interdisciplinary research projects combining applied mathematics, physiology and several areas of engineering. It has become widely accepted that techniques from applied mathematics - in particular from the areas of optimization and numerical mathematics - are essential for extending our scientific knowledge and thus contributing significantly to the solution of problems which are of concern to our society. The interdisciplinary efforts within the SRC lead to innovative solutions to solve such problems. The SRC also provides the necessary scientific environment and training for young researchers to cooperate in similar research projects. The SRC F-003 is supported by the Austrian Science Fund. The sponsoring subprojects for the workshop were:

- F310: Optimization of a mathematical model for fundamental control mechanisms in the cardiovascular system.
- F312: Identification of models of the adaptation of the heart function to the demands of the cardiovascular and cardiorespiratory system.
- F323: Optimization of Fluid Balance: Blood pressure control and clinic applications such as hemodialysis.